

Water Resources Research

RESEARCH ARTICLE

10.1029/2024WR037538

Special Collection:

Hydrogeodesy: Understanding changes in water resources using space geodetic observations

Key Points:

- A novel joint inversion model is established from joint adjustment of Gravity Recovery and Climate Experiment (GRACE)-based geopotential differences and Global Navigation Satellite System (GNSS) vertical displacements
- Joint inversion demonstrates superior performances compared to GRACE- and GNSS-only solutions through closed-loop simulations
- Joint inversion results show better consistency with in situ data than GRACE- and GNSS-only solutions at monthly and weekly scales in Brazil

Supporting Information:

Supporting Information may be found in the online version of this article.

Correspondence to:

X. Li,
lixianpao@whu.edu.cn


Citation:

Zhong, B., Li, X., Chen, J., Li, J., & Xu, H. (2024). Estimation of terrestrial water storage changes in Brazil from the joint inversion of GRACE-based geopotential difference and GNSS vertical displacement data. *Water Resources Research*, 60, e2024WR037538. <https://doi.org/10.1029/2024WR037538>

Received 20 MAR 2024

Accepted 20 OCT 2024

Estimation of Terrestrial Water Storage Changes in Brazil From the Joint Inversion of GRACE-Based Geopotential Difference and GNSS Vertical Displacement Data

Bo Zhong^{1,2} , Xianpao Li¹ , Jianli Chen^{3,4,5} , Jiancheng Li^{1,2}, and Hongyi Xu¹

¹MOE Key Laboratory of Geospace Environment and Geodesy, School of Geodesy and Geomatics, Wuhan University, Wuhan, China, ²Hubei LuoJia Laboratory, Wuhan, China, ³Department of Land Surveying and Geo-Informatics, The Hong Kong Polytechnic University, Hong Kong, China, ⁴Research Institute for Land and Space, The Hong Kong Polytechnic University, Hong Kong, China, ⁵Shenzhen Research Institute, The Hong Kong Polytechnic University, Shenzhen, China

Abstract Gravity Recovery and Climate Experiment (GRACE) satellite gravimetry and Global Navigation Satellite System (GNSS) surface displacement measurements offer complementary advantages for monitoring terrestrial water storage (TWS) changes. We propose a new joint inversion model based on the combination of GRACE-based geopotential difference (GPD) observations using the mascon method and GNSS vertical displacements through the Green's function method to obtain reliable TWS changes in Brazil. The performance of the jointly inverted TWS changes is assessed through closed-loop simulations and comparisons with hydrometeorological data (precipitation-P, evapotranspiration-ET, and runoff-R) using water budget closure (P-ET-R) and river water level observations from satellite altimetry. The simulation results indicate that the joint inversion results exhibit higher accuracy and reliability than GRACE GPD-based mascon (GPD-mascon) and GNSS solutions, and the standard deviations (STDs) of joint results decrease by ~6.98 and ~37.5 mm compared to those from GPD-mascon and GNSS solutions. The joint inversion of real GRACE and GNSS data demonstrates notably lower uncertainty than that of GPD-mascon solutions and exhibits significant improvement than GNSS-only solutions. The STDs and correlation coefficients between monthly R time series derived from three inversion methods (joint inversion, GPD-mascon and GNSS solutions, combined with P and ET through water budget closure) and in situ observations are 19.607 mm and 0.912, 20.879 mm and 0.904, and 31.370 mm and 0.778, respectively. The joint estimates also yield better correlation with river water level observations compared to GPD-mascon and GNSS solutions. Furthermore, at the weekly time scale, the joint inversion results show better consistency with P-ET-R data than those from GPD-mascon and GNSS solutions.

Plain Language Summary The migration and redistribution of surface mass changes (e.g., TWS changes) can induce changes in the Earth's gravity field and surface deformation field. The remote sensing-based Gravity Recovery and Climate Experiment (GRACE) satellite gravimetry and ground-based Global Navigation Satellite System (GNSS) displacement measurement complement each other in spatio-temporal resolution, spectral sensitivity, and spatial coverage for retrieving TWS changes. We present a novel joint inversion model that estimates reliable monthly and weekly TWS changes in Brazil through the joint adjustment of GRACE-based geopotential differences (GPDs) and GNSS vertical displacements based on the mascon method and Green's function method in the spatial domains at the observation level. Compared to the GRACE-only (GPD-mascon) and GNSS-only solutions, the joint inversion can recover more reliable TWS changes in Brazil through closed-loop simulation tests. In addition, the joint inversion results based on the measured data present better consistency with hydrometeorological variables and river water level time series than GPD-mascon and GNSS solutions. The proposed approach provides an effective estimation strategy to combine multi-source geodetic data (e.g., GRACE/GRACE-FO and GNSS) for recovering reliable TWS changes, which can provide crucial data support for studying water cycles and extreme climate events.

1. Introduction

Global climate change and anthropogenic activities exert growing influences on water resource variations. The impact of climate change is evident in the rise of extreme climate events (e.g., floods, droughts, and hurricanes), directly impacting the distribution and accessibility of water resources (Lehner et al., 2006; Pokhrel et al., 2021). Meanwhile, the global trends of population growth, urbanization, and industrialization have accelerated the demand for water resources, presenting formidable challenges to water resource management. Terrestrial water

© 2024. The Author(s).

This is an open access article under the terms of the [Creative Commons Attribution License](https://creativecommons.org/licenses/by/4.0/), which permits use, distribution and reproduction in any medium, provided the original work is properly cited.

storage (TWS) change is one of the key indicators of water resources, and accurate quantification of the spatio-temporal distribution characteristics and evolution patterns of TWS changes is crucial for the rational allocation of water resources and the sustainable development of the socio-economic systems (Huang et al., 2021; Tapley et al., 2019).

The redistribution of TWS can induce changes in both the Earth's gravity field and the surface displacement field. Since March 2002, the Gravity Recovery and Climate Experiment (GRACE) and GRACE Follow-on (GRACE-FO) satellite missions have provided crucial technical support for monitoring the time-variable gravity fields (Tapley et al., 2019). The gravity field products derived from GRACE/GRACE-FO can be utilized to detect terrestrial water cycling (e.g., Humphrey et al., 2016; Syed et al., 2008), polar and high-mountain glaciers melting (e.g., Chen et al., 2006; Jacob et al., 2012), groundwater depletion (e.g., Feng et al., 2013; Rodell et al., 2009), sea level changes (e.g., Cazenave et al., 2009; Chambers, 2006; Chen et al., 2018), as well as investigate extreme climate events (e.g., floods and droughts) related to water variations (e.g., Long et al., 2013; Thomas et al., 2014). In addition, over the past decade, the use of the Global Navigation Satellite System (GNSS) to monitor surface displacement for tracking TWS changes according to loading Green's function theory (Farrell, 1972) has garnered increasing attention (e.g., Argus et al., 2014; Borsa et al., 2014; White et al., 2022). Similar to GRACE/GRACE-FO observations, the TWS changes inferred through GNSS inversion are also applicable for regional water cycling (Enzminger et al., 2019; Zhang & Jin, 2016) and monitoring extreme climate events (Borsa et al., 2014; Jiang et al., 2022; Milliner et al., 2018; Zhu, Chen, Hu, Liu, et al., 2023). This approach has gained widespread uses in regions such as North America (Argus et al., 2014; Enzminger et al., 2018; Fu et al., 2015), China (Jiang et al., 2021; Li et al., 2023a, 2023b), South America (Ferreira et al., 2019; Jiang et al., 2022), and Australia (Han & Razeghi, 2017). A comprehensive review of inverting GNSS surface displacement observations for TWS changes and its applications in the hydrogeodesy field is available in White et al. (2022).

However, limited by the satellite orbit height and configuration, observation accuracy, uncertainties in background field models, and other error sources, TWS changes estimated by GRACE/GRACE-FO are usually presented at the temporal resolution of monthly scale and the spatial resolution of ~300–500 km (e.g., Kim et al., 2024; Tapley et al., 2019). These shortages limit the usage of GRACE/GRACE-FO for monitoring TWS changes at high spatio-temporal resolution (e.g., sub-monthly and localized scales). However, GNSS can continuously monitor surface displacements in near-real-time (e.g., daily scale) with millimeter-level observation accuracy, which is more sensitive to regional and localized TWS changes compared to GRACE/GRACE-FO (Bevis et al., 2005). For instance, the spatial resolution of GNSS-recovered TWS changes can reach ~50 km in California (Argus et al., 2014), where the GNSS stations are densely distributed. Nevertheless, since there are no GNSS stations distributed in the ocean area (accounting for ~71% of the global area), it is challenging to invert the globally distributed GNSS observations to recover the high-degree spherical harmonic (SH) coefficients corresponding to global TWS changes.

Considering the complementary strengths of GRACE/GRACE-FO and GNSS in terms of spatio-temporal resolution, spatial coverage, and spectral sensitivity, previous publications jointly inverted the GRACE/GRACE-FO and GNSS observations to obtain more reliable TWS changes. There are two commonly used joint inversion methods for retrieving TWS changes. One is to recover global SH coefficients in the spectral domain (Kusche & Schrama, 2005; Razeghi et al., 2019; Rietbroek et al., 2012; X. Wu et al., 2006). For example, Kusche and Schrama (2005) introduced a physically motivated regularization method to stabilize the joint inversion results from GNSS surface displacements and GRACE monthly gravity field solutions. The results showed that jointly inverted TWS changes present good consistency with GRACE-only and hydrological model outputs, and the contributions of GNSS to the degree 2 to degree 4 SH coefficients exceed 60%, and the corresponding contributions to SH coefficients beyond degree 4 exceed 30%. Following the method of Kusche and Schrama (2005), Wu et al. (2006) jointly inverted GNSS displacement time series at nearly 450 stations, ocean bottom pressure (OBP) models, and GRACE monthly gravity field models to obtain the SH coefficient solutions complete to degree and order 50. Furthermore, Razeghi et al. (2019) implemented a joint inversion framework for the co-estimation of geocenter motion and gravitational potential SH coefficients up to degree 90 through the joint analysis of GNSS displacements and GRACE geopotential data, the results demonstrated that the inclusion of GNSS in the joint inversion framework significantly enhances the reliability of TWS changes in major basins in the United States and Europe. Although the joint inversion for SH coefficients in the spectral domain has improved the spatial resolution and reliability of estimated TWS changes to some extent, the potentials of GRACE and GNSS in monitoring fine-scale regional TWS changes have not been effectively utilized.

To enhance the computational efficiency of joint inversion and better utilize the advantages of GNSS in monitoring regional water loading, another joint inversion method that jointly inverts the GRACE and GNSS observations for regional TWS changes in the spatial domain has garnered increasing attention in recent years (e.g., Adusumilli et al., 2019; Argus et al., 2022; Carlson et al., 2022; Fok & Liu, 2019; Li et al., 2023a, 2024; Yang et al., 2023; Zhu, Chen, Hu, Wei, et al., 2023). For instance, Adusumilli et al. (2019) utilized the GRACE mass concentration (mascon) grid products to constrain the GNSS-inverted TWS changes, and the joint estimates presented better spatial resolution than GRACE-only solutions. Fok and Liu (2019) introduced the GRACE SH solutions derived vertical displacements at some “virtual” stations (used to establish the observation equation between GRACE-derived displacements and TWS changes) into the GNSS-only inversion model to enhance the reliability of GNSS-inverted TWS changes. Additionally, to better integrate the respective advantages of GNSS and GRACE/GRACE-FO, Carlson et al. (2022) used a continuous wavelet transform to decompose GNSS and GRACE/GRACE-FO observations for joint inversion, and the joint results showed improved spatial resolution of TWS changes than GRACE in California. Yang et al. (2023) reported that the TWS changes from the joint inversion of vertical displacements at “virtual” stations derived from GRACE/GRACE-FO and observed by GNSS are more reliable than those using the GRACE/GRACE-FO mascon grid products to constrain the GNSS-only inversion results.

Our previous studies also focused on the joint inversion of GNSS and GRACE/GRACE-FO and land surface model for estimating reliable TWS changes. For example, Li et al. (2023a) investigated the performance of two commonly used weighting strategies (i.e., variance component estimation [VCE] and Akaike's Bayesian Information Criterion [ABIC]) for determining the relative weights of the joint inversion of GNSS-observed and GRACE-derived vertical displacements in the Yangtze River basin of China, and the results indicated that the ABIC is superior to VCE in the joint inversion model. Li et al. (2023b) utilized the land surface model-derived covariance matrix to replace the commonly used Laplacian matrix to constrain the GNSS-only inversion results for retrieving reliable TWS changes, and this inversion strategy fundamentally involved a joint inversion of GNSS and land surface models. Furthermore, Li et al. (2024) used the GRACE/GRACE-FO mascon grid products as the a priori information and employed the corresponding covariance matrix as the regularization constraints to stabilize the GNSS-only inversion results, and the reliable TWS changes from the joint inversion were used to effectively reveal the extreme droughts and floods in Sichuan Province of China. Although these joint inversion results demonstrate certain advantages compared to GRACE- and GNSS-only solutions, there are still some issues that require further in-depth investigations: (a) for the joint inversion of GNSS-observed and GRACE-derived vertical displacements, the spatial distribution of “virtual” stations for GRACE observations cannot be reasonably determined, (b) for using the GRACE mascon grid products to constrain the GNSS inversion results, the joint inversion model can easily overfit the GNSS observations (Yang et al., 2023), (c) the jointly inverted TWS changes provided by the majority of previous publications have temporal resolution at monthly scales, which sacrifices the advantages of high time resolution of GNSS observations.

Compared to K-band ranging range (KBRR) geometric observations, the GRACE-derived geopotential difference (GPD) is a physically meaningful variable (Han et al., 2006; Shang et al., 2015) and has the advantage of establishing a linear relationship with surface mass changes (Han et al., 2005; Zhong et al., 2020), which is simpler and more computationally efficient compared to the official dynamic method. Meanwhile, the GPD data are fully publicly accessible at Zhong et al. (2022), and researchers can easily develop monthly, weekly, or even daily TWS changes for any study region using the GRACE-based GPD data as needed. This study introduces a rigorous solution method for jointly inverting GRACE L1b data estimated GPDs and GNSS vertical displacements for regional TWS changes at the observation level. To capture the same benefits as GRACE mascon solutions (Loomis et al., 2019; Save et al., 2016; Watkins et al., 2015), the GPD-based mascon (GPD-mascon) method (Han et al., 2005; Ramillien et al., 2011; Tangdamrongsub et al., 2012; Zhong et al., 2020, 2023) was utilized to directly establish the mathematical relationship between GPD observations and TWS changes in the spatial domain, which can offer higher computational efficiency and easily introduce external constraints to stabilize the solutions compared to the traditional SH basis function method. Meanwhile, the Green's function method (Argus et al., 2014; Farrell, 1972) in the spatial domain inversion rather than the Slepian basis function method in the spectral domain inversion (Han & Razeghi, 2017) was used to establish a mathematical relationship between GNSS vertical displacements and TWS changes. Furthermore, normal equations of the GPD-mascon and Green's function methods were combined based on the joint adjustment method in a more rigorous sense. We chose Brazil as a case study region (Figure 1a), which possesses abundant water resources (including the Amazon

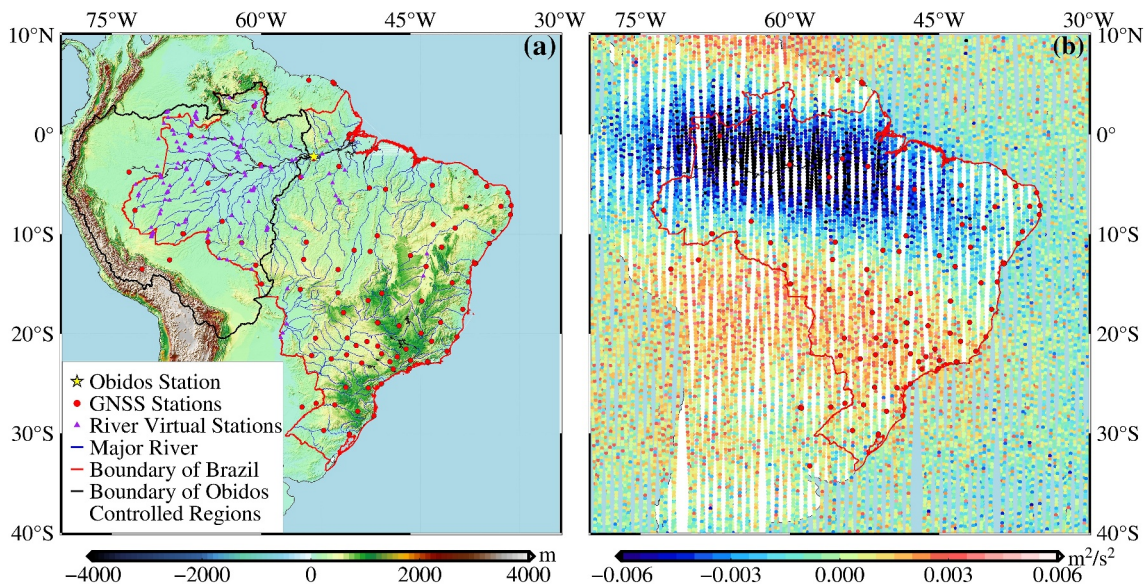


Figure 1. (a) Overview of the topography and spatial distribution of GNSS stations (red dots), river virtual stations (purple triangles), and the Obidos hydrological station (yellow five-pointed star) in Brazil. The red and black curves represent the boundaries of Brazil and the watersheds controlled by Obidos station, and the blue curves outline the major rivers; (b) the spatial distribution of GRACE-based geopotential difference (GPD) residual observations in August 2008.

basin) and a diverse range of climatic types (e.g., tropical rainforest, subtropical, and arid climates), as well as the GNSS stations distributed with different densities, making it particularly suitable for validating the performance of our proposed joint inversion model. Therefore, the primary objectives of the present study are (a) utilizing a more rigorous joint inversion method than previous works to jointly invert GRACE-based GPD observations and GNSS vertical displacements for regional TWS changes, (b) establishing stable and reliable TWS change time series model through the joint inversion of GRACE and GNSS observations, and for the first time, constructing weekly TWS changes in Brazil, and (c) employing hydrometeorological data from multiple sources, including land surface model, reanalysis data, and in situ measurements, along with river water level time series obtained from satellite altimetry, to validate the superiority of the jointly inverted TWS changes over GRACE- and GNSS-only inversion results.

The remaining sections of this study are organized as follows: Section 2 introduces the data sets and the corresponding post-processing procedures. Section 3 presents the fundamental theory, inversion models, and research framework of this study. Section 4 validates the performance of joint inversion model through closed-loop simulation, official GRACE mascon and SH solutions, as well as independent hydrometeorological data and river water level time series. Finally, the conclusions are summarized in Section 5.

2. Study Region and Materials

2.1. Study Region

Brazil (35°–74°W and 35°S–5°N, Figure 1a) is the largest country in South America, with a total area of ~8.5 million km². The terrain of Brazil is primarily composed of plateaus and plains, the Amazon basin in the north and the Brazilian plateau in the south occupy one-third and two-thirds of the country's land area, respectively. Most regions of Brazil lie between the Equator and the Tropic of Capricorn, and its climate types are predominantly tropical rainforest (Amazon basin) and tropical savanna (Brazilian plateau), making it the country with the largest tropical area. In addition, Brazil has rich water resources, especially, the total river flow of Amazon river surpasses the combined flow of the next seven largest rivers, accounting for about 20% of the world's total river discharge into the oceans (Chen et al., 2020). Therefore, accurate quantization of the spatio-temporal evolutions of TWS changes in Brazil is crucial for global and regional water cycle. It is noteworthy that the ground-based GNSS surface displacement observations and satellite-based remote sensing observations (e.g., GRACE/GRACE-FO) provide important technical support for monitoring water resources in this region. Meanwhile, the water loading signals outside Brazil are not significant, therefore, it is particularly suitable for validating the

performance of different observation techniques and inversion algorithms in monitoring water resources. To reduce the edge effects of the recovered TWS changes, we extended the actual calculation area to 26.5°–82.5°W and 41.5°S–13.5°N. Furthermore, since GNSS measurement is primarily driven by the mass loading changes within a distance of ~100 km (Bevis et al., 2005), the GNSS stations within 3° of the Brazilian boundary were used for the inversion.

2.2. Simulation Data

A closed-loop simulation was conducted before the inversion of measured data. In this study, we utilized the Earth System Model (ESM) AOHIS (Atmosphere, Ocean, Hydrology, Ice, Solid Earth) and DEAL+AOerr time-varying SH products (Dobslaw et al., 2015) spanning from January 2004 to December 2006 for simulation analysis. The HIS signals (sum of Hydrology, Ice, and Solid Earth) were set to the “true” hydrological loading signals, and the differences between the AOHIS and DEAL+AOerr SH coefficients were used to generate the simulated GRACE-based GPD and GNSS vertical displacement observations, which consider aliasing errors of atmospheric and oceanic effects corrected by external geophysical models.

2.3. GRACE Geopotential Difference Data

In the present study, the GRACE-based GPD data (Zhong et al., 2022) from January 2008 to July 2016 were used to recover the monthly and weekly TWS changes in Brazil. The GRACE-based GPD data were generated using GRACE Level-1b (RL03) data and the latest data processing standards (Bettadpur, 2018), and the improved energy balance equation and remove-compute-restore (RCR) technique were utilized to improve the estimation accuracy of GPD data (Zhong et al., 2020). For a comprehensive understanding of the data processing techniques and procedures applied to obtain the GRACE-based GPD data, please refer to our previous publications (Zhong et al., 2020, 2022, 2023). Figure 1b presents the spatial distributions of residual GPD observations in August 2008, which are the direct reflection of surface mass changes. It can be seen that the abundant GPD observations can be used as a useful supplement to ground-based GNSS observations in Brazil (especially in the Amazon basin), which provide good data support for the joint inversion of GNSS and GRACE data to obtain reliable TWS changes in the studied region.

2.4. GRACE Mascon and SH Solutions

Monthly GRACE Release-06 (RL06) mascon solutions published by the Center for Space Research (CSR) (Save et al., 2016), Jet Propulsion Laboratory (JPL) (Watkins et al., 2015), and Goddard Space Flight Center (GSFC) (Loomis et al., 2019), as well as the monthly SH coefficient solutions (complete to degree and order 60) from CSR and weekly SH coefficient solutions (complete to degree and order 30) published by GeoforschungsZentrum Potsdam (GFZ) were used to assess the performance of the joint inversion results. It should be emphasized that the mascon solutions suppress the north-south striping errors of GRACE observations through the adoption of external constraint information, providing higher spatial resolution compared to unconstrained SH solutions. Consequently, the mascon products can be used to infer TWS changes without any additional filtering and signal leakage corrections. The grid sizes of CSR, JPL, and GSFC mascon products are $0.25^\circ \times 0.25^\circ$, $0.5^\circ \times 0.5^\circ$, and $0.5^\circ \times 0.5^\circ$ grids, respectively, while the real spatial resolution of mascon solutions is still limited by the native resolution of GRACE observations (i.e., ~300 km). For the CSR and GFZ SH coefficient solutions, the 300 km Gaussian filtering (Wahr et al., 1998) plus P3M6 de-striping filtering (Chen et al., 2007) were used to derive the TWS changes over Brazil. Moreover, due to significant uncertainties in the low-degree SH coefficients (e.g., C_{20} term) solved from the GRACE observations, various corrections were implemented during this data processing of the mascon and SH solutions. The C_{20} terms were replaced by the estimates derived from Satellite Laser Ranging (SLR) (Loomis et al., 2020), and the degree-1 terms (i.e., geocenter) and glacial isostatic adjustment (GIA) effects were corrected using the supplementary data sets (GRACE Technical Note 13) (Landerer, 2019) from the GRACE project and ICE-6G_D model (Peltier et al., 2018), respectively. In particular, the GRACE CSR SH solutions were not corrected for GIA effects when comparing the GNSS-monitored and GRACE CSR SH solutions calculated vertical displacements, this is because the original GNSS vertical displacement time series include the GIA effects.

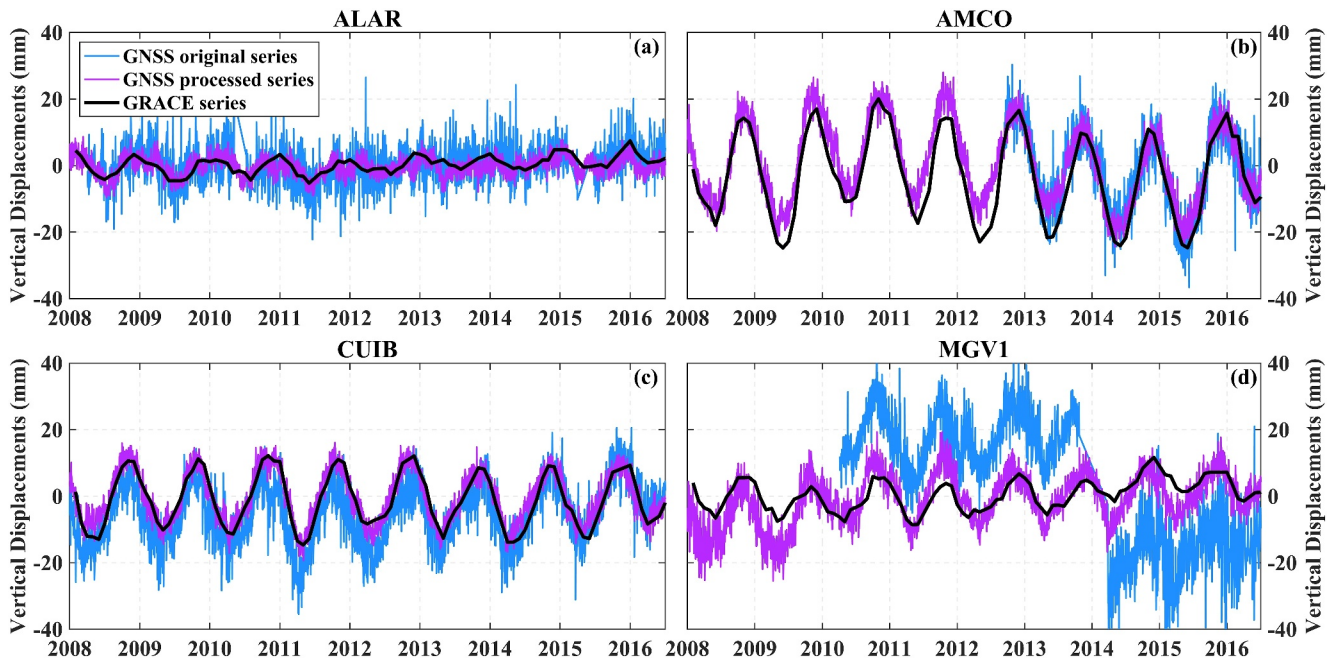


Figure 2. Vertical displacement time series derived from GNSS (before and after post-processing) and GRACE CSR spherical harmonic (SH) coefficient solutions in four selected stations ((a) ALAR, (b) AMCO, (c) CUIB, and (d) MGVI) in Brazil from January 2008 to July 2016.

2.5. GNSS Vertical Displacement Time Series

Daily GNSS vertical displacement time series from January 2008 to July 2016 at 103 stations (red dots in Figure 1a), provided by the Nevada Geodetic Laboratory (NGL) (Blewitt et al., 2018), were used to recover the TWS changes in Brazil. These published time series were processed by using the GipsyX version 1.0 software, released by the JPL, with precise point positioning technology. For details of the GNSS data processing strategies, see <http://geodesy.unr.edu/gps/ngl.acn.txt>. Due to the influences of human activity, natural environment, equipment maintenance, and other factors, there are data gaps, steps, outliers, and high-frequency noises in the GNSS vertical displacement time series. To this end, we conducted various corrections for the original GNSS vertical displacement observations to obtain continuous and reliable vertical displacement time series associated with water loading for joint inversion. First, we employed the TSAlyzer software developed by D. Wu et al. (2017) to eliminate the steps and used the quartile gross error detection method to remove the outliers. Second, we used the principal component analysis (PCA) method to interpolate missing information, and the first eight principal components were used to reconstruct the GNSS vertical displacement time series. Third, we employed the fluid loading products associated with the non-tidal atmospheric and oceanic loading published by the Earth System Modeling group at GFZ (Dill & Döbslaw, 2013) to correct the non-tidal atmospheric and oceanic loading effects. Finally, the long-term trend of GNSS observations includes the comprehensive contributions of the GIA, tectonic effects, and TWS changes. However, isolating the precise contributions of these components to long-term trends proves challenging. Figure S1 in Supporting Information S1 compares the long-term trends of vertical displacement time series at 103 stations derived from GNSS observations and GRACE products (considered from the GRACE CSR SH solutions), indicating that there are differences in the amplitude or direction of long-term trends estimated by GNSS and GRACE at most stations. These differences are primarily caused by tectonic movements, which are not included in the GRACE observations. Therefore, to mitigate the impact of tectonic deformation on the inverted TWS changes from GNSS displacement time series, we utilized the long-term trend of vertical displacement time series at 103 GNSS stations derived from GRACE, to replace the original long-term trend of GNSS vertical displacement time series before inversion.

Figure 2 illustrates the comparison of the vertical displacement time series derived from GNSS before and after post-processing and from GRACE CSR SH coefficient products (please refer to van Dam et al. (2007)) at ALAR (with significant high-frequency noises), AMCO (with significant missing data), CUIB (with good data quality), and MGVI (with significant steps) stations. As illustrated in Figure 2, our post-processing strategies well handle

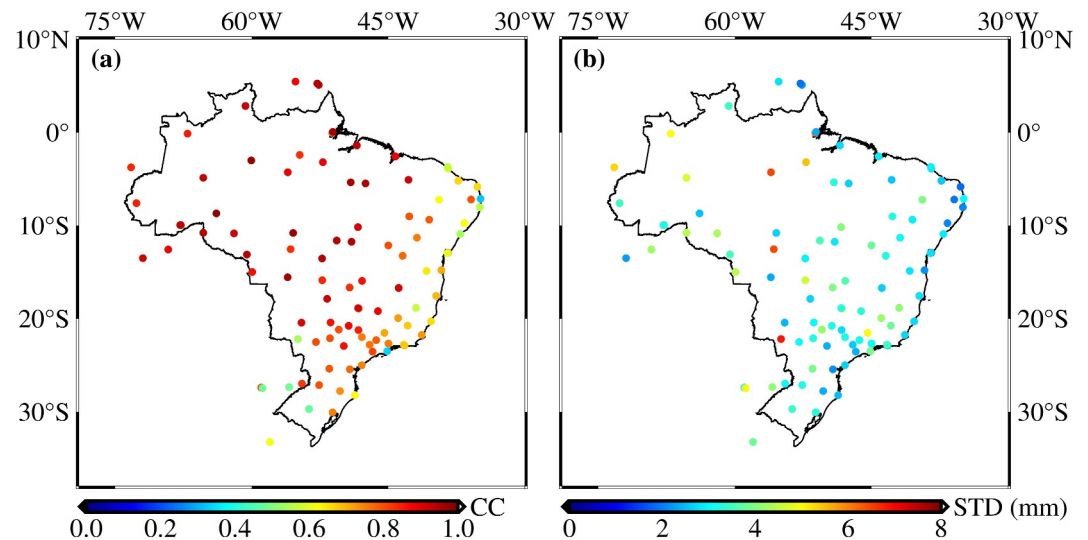


Figure 3. Values of (a) correlation coefficient (CC) and (b) standard deviation (STD) between the GNSS-observed and GRACE-derived vertical displacement time series at 103 GNSS stations in Brazil from January 2008 to July 2016.

the data gaps, steps, outliers, and high-frequency noises of the GNSS vertical displacement time series, and the processed GNSS time series present good consistency with the GRACE SH solutions. Figure 3 reveals the values of correlation coefficient (CC) and standard deviation (STD) between the GNSS-observed and GRACE-derived monthly vertical displacement time series at the 103 stations in Brazil. As revealed in Figure 3, the consistency between GNSS and GRACE observations in the marginal area of Brazil near the Atlantic Ocean is generally worse than that in the inland area, which may be caused by signal leakages of GRACE SH solutions. The minimum and maximum correlations occurred in PBJP (CC = 0.32) and POVE (CC = 0.98) stations, and the average value of CCs for the 103 stations is approximately 0.79. Meanwhile, the minimum and maximum STDs occurred in RNNA (STD = 1.83 mm) and LSTM (STD = 18.15 mm) stations, and the average value of STDs for the 103 stations is approximately 3.54 mm. In general, the vertical displacement time series derived from GNSS and GRACE maintain good consistency with each other, while the signal amplitudes of GNSS and GRACE estimates still present differences, which are mainly caused by the differences in spatio-temporal resolution, spatial coverage, and spectrum sensitivity of GNSS and GRACE observation technologies.

2.6. Hydrometeorological Data

We used hydrometeorological data, including precipitation (P), evapotranspiration (ET), and runoff (R) derived from the European Centre for Medium-Range Weather Forecasts (ECMWF) ERA5 reanalysis data (Muñoz Sabater, 2019), Global Land Data Assimilations System (GLDAS)-Noah (version 2.1) land surface model outputs (Rodell et al., 2004), and WaterGAP Global Hydrology Model (WGHM) hydrological model products (Müller et al., 2021) to validate the performance of TWS changes inverted from multisource geodetic observations. Figure 4 shows the comparisons of P, ET, and R time series derived from ERA5, GLDAS, and WGHM from January 2008 to July 2016 in Brazil. As shown in Figure 4, all of these time series present significant seasonality during the study period, and the consistency among the P time series is the best, followed by the R, and the ET is the worst. Among them, the CC values between these three P time series are greater than 0.994 and STD values are 7.04–8.05 mm/month [mon], and the corresponding values for R time series are 0.91–0.98 and 8.67–17.07 mm/mon and for ET time series are 0.83–0.94 and 13.82–40.35 mm/mon, respectively. Meanwhile, we also collected the in situ R time series at the Obidos hydrological station (see the location of the yellow five-pointed star in Figure 1a; the data is available at <https://hybam.obs-mip.fr>) for comparison. In this work, the P, ET, and R time series were converted into the first order derivative of TWS changes (dS) via the water budget closure method (Chen et al., 2020) as follows:

$$dS = P - ET - R \quad (1)$$

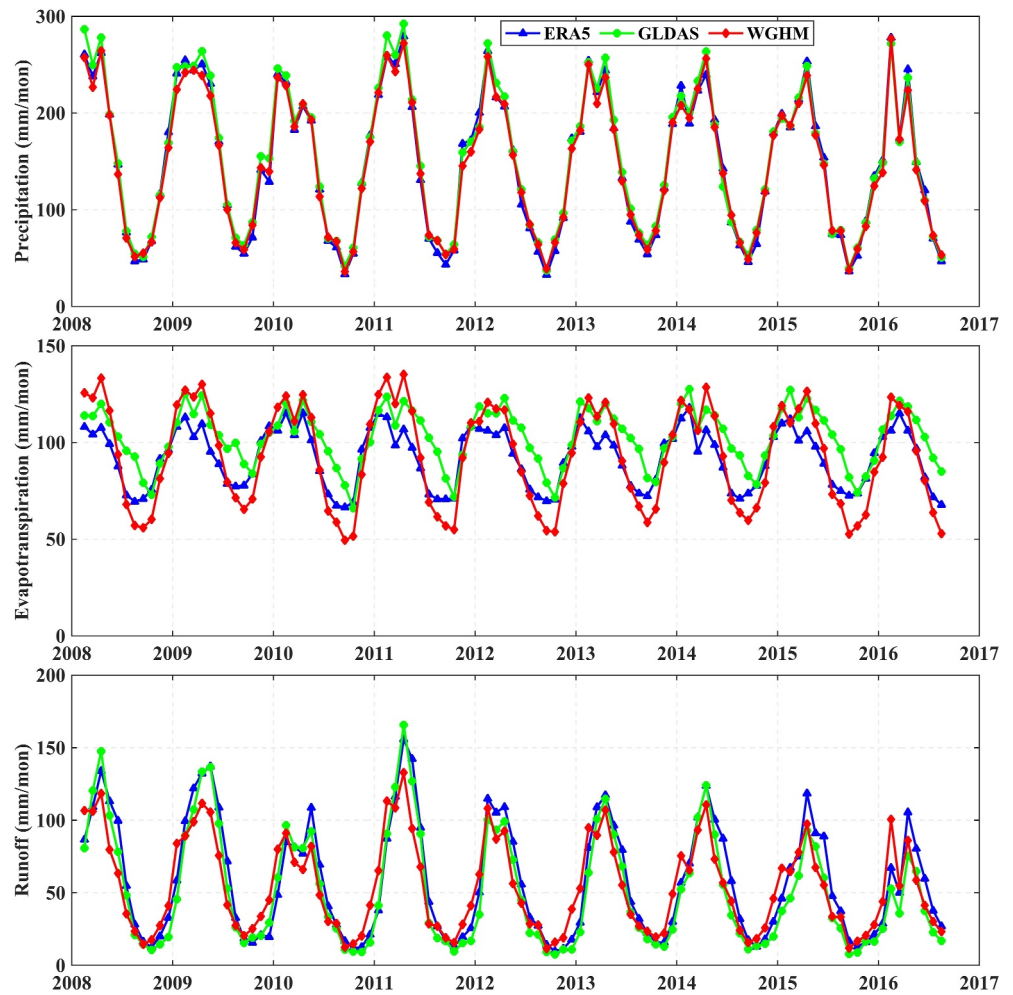


Figure 4. Precipitation, evapotranspiration, and runoff time series derived from ERA5, GLDAS, and WGHM in Brazil from January 2008 to July 2016.

Note that the epoch of dS time series from P, ET, and R in Equation 1 is in the middle of the month, while the corresponding value of first order derivative of TWS (dS_t/dt) time series derived from geodetic data (e.g., GNSS and GRACE) is at the start (or end) of the month. To maintain the time consistency of the dS time series, we interpolated the dS_t/dt time series at the middle of the month through cubic spline interpolation.

In addition to the P, ET, and R time series derived from model products and in situ measurements, the river water level time series in Brazil derived from the ERS 2 and ENVISAT radar altimetry missions (Silva et al., 2010) were also used for evaluation. There are a total of 5,077 river water level “virtual” stations in Brazil, however, most of them (4,060 stations) started monitoring the river water level after 2016, which cannot be used to assess the TWS changes in Brazil during the study period. In this study, to ensure that there are at least 36 observation values in the river water level time series at the “virtual” station during the study period for correlation analysis with TWS changes, a total of 162 “virtual” stations were selected for evaluation (see the purple triangles in Figure 1a). Note that there are 160 stations located in northwestern Brazil, with only two stations located in the southeastern Brazil.

3. Methods

3.1. GPD-Based Mascon Inversion Model

The mascon method enables a direct establishment of the mathematical relationship between the mass blocks of the studied region and GRACE L1b observations (e.g., KBRR and GPD data). In this study, we used the GRACE-based GPD observations to recover regional TWS changes in Brazil, the relationship between the GPDs (T_{AB}) and

TWS changes, as dictated by Newton's law of universal gravitation, can be described as follows (Han et al., 2005; Ramillien et al., 2011; Zhong et al., 2023):

$$\begin{cases} T_{AB} = G \sum_{j=1}^M \left(\frac{1}{l_B^j} - \frac{1}{l_A^j} \right) \delta m_j \\ \frac{1}{l_{A,B}^j} = \frac{1}{R} \sum_{l=0}^{\infty} \left(\frac{R}{r_{A,B}} \right)^{l+1} P_l(\cos \psi_{A,B}^j), R < r_{A,B} \end{cases} \quad (2)$$

in which G is the Newtonian gravitational constant ($6.673 \times 10^{-11} \text{ m}^3 \text{ kg}^{-1} \text{ s}^{-2}$), R is the average equatorial radius of the Earth (6,378,136.3 m), M indicates the number of the grids within the calculated region; $\delta m_j = \rho_w \delta S_j \delta h_j$ represent the mass of TWS changes in the j th grid cell, δS_j and δh_j are the area and equivalent water height (EWH) of the j th grid cell; l_A^j and l_B^j denote the distances between the GRACE satellites A , B and the center of the j th grid cell; r_A and r_B are the geocentric radii of GRACE satellites A , B ; ψ_A^j and ψ_B^j are the geocentric angles between GRACE satellites A , B and the j th grid cell; P_l are the Legendre polynomials of order l .

Following Equation 2 and taking into account the loading effects resulting from TWS changes, the observation equation connects the GPD observations and TWS changes can be expressed as follows (Ramillien et al., 2011; Zhong et al., 2023):

$$T_{AB} = \frac{G\rho_w}{R} \sum_{j=1}^M \sum_{l=0}^{\infty} \delta S_j \delta h_j (1 + k_l) \left(\left(\frac{R}{r_B} \right)^{l+1} P_l(\cos \psi_B^j) - \left(\frac{R}{r_A} \right)^{l+1} P_l(\cos \psi_A^j) \right) \quad (3)$$

in which ρ_w denotes the density of fresh water ($1,000 \text{ kg/m}^3$) and k_l represent the loading Love numbers associated with the elastic deformation potential for a viscoelastic Earth (H. Wang et al., 2012).

The linear model of Equation 3 can be formulated as follows:

$$\mathbf{y}_1 = \mathbf{A}_1 \mathbf{x} + \mathbf{e}_1, \quad \mathbf{e}_1 \sim (0, \sigma_{y_1}^2 \mathbf{I}_{y_1}) \quad (4)$$

where $\mathbf{y}_1 = \{T_{AB,i}\}_{i=1,2,\dots,n_1}$ indicates the vector of GPD observations, and n_1 represents the total number of GPD observations; \mathbf{A}_1 is the design matrix derived from Equation 3; $\mathbf{x} = \{\delta h_j\}_{j=1,2,\dots,M}$ is the TWS change vector (expressed in EWH) needs to be estimated; \mathbf{e}_1 and $\sigma_{y_1}^2$ signify the observation error vector and error variance of GPD observations; \mathbf{I}_{y_1} is the identity matrix corresponding to the length of \mathbf{y}_1 .

To improve the stability of the GPDs estimated TWS changes (i.e., \mathbf{x}), we introduced a stochastic model for the \mathbf{x} as the a priori information. The a priori constraint equation can be formulated as follows:

$$\mathbf{x}_0 = \mathbf{I}_x \mathbf{x} + \mathbf{e}_0, \quad \mathbf{e}_0 \sim (0, \mathbf{C}_x) \quad (5)$$

where \mathbf{x}_0 represents the priori expectation vector of unknown TWS changes, which is deliberately set to 0 to reduce the influence from external information; \mathbf{I}_x is the identity matrix corresponding the length of \mathbf{x} ; \mathbf{e}_0 is the residual vector characterized by zero expectation and covariance matrix \mathbf{C}_x , the specific calculation method can be found in previous publications (Ferreira et al., 2023; Tangdamrongsub et al., 2012; Zhong et al., 2020).

The objective function of the GRACE-only inversion model is as follows:

$$\min \left\{ \left\| \frac{\mathbf{A}_1 \mathbf{x} - \mathbf{y}_1}{\sigma_{y_1}} \right\|^2 + \alpha \|\mathbf{x} - \mathbf{x}_0\|^2 \right\} \quad (6)$$

in which α represents the regularization parameter that balances the relative contributions between the GPD observations and constraint matrix.

By combining Equation 4 and Equation 5, the least-squares solutions of the unknown TWS change vector can be estimated as follows:

$$\hat{\mathbf{x}} = (\mathbf{A}_1^T \mathbf{A}_1 + \alpha \sigma_{y_1}^2 \mathbf{C}_x^{-1})^{-1} (\mathbf{A}_1^T \mathbf{y}_1 + \alpha \sigma_{y_1}^2 \mathbf{C}_x^{-1} \mathbf{x}_0) \quad (7)$$

Due to the $\sigma_{y_1}^2$ estimated from observational data in Equation 6 is not entirely accurate, we can concurrently solve the product of α and $\sigma_{y_1}^2$ (i.e., $\alpha \sigma_{y_1}^2$) using the VCE method (Koch & Kusche, 2002):

$$\hat{\alpha \sigma_{y_1}^2} = \frac{\mathbf{y}_1^T \mathbf{y}_1 - \hat{\mathbf{x}}^T (2\mathbf{A}_1^T \mathbf{y}_1) + \hat{\mathbf{x}}^T (\mathbf{A}_1^T \mathbf{A}_1) \hat{\mathbf{x}}}{n_1 - (\mathbf{x}_0 - \hat{\mathbf{x}})^T \mathbf{C}_x^{-1} (\mathbf{x}_0 - \hat{\mathbf{x}})} \quad (8)$$

3.2. GNSS-Only Inversion Model

According to the theory of elastic loading (Farrell, 1972), the deformation of the Earth induced by changes in surface mass changes (e.g., surface water, glaciers, and atmospheric pressure) can be approximately expressed as elastic deformation, encompassing both vertical and horizontal displacements. Since vertical displacement is more sensitive to mass loading compared to horizontal displacement (Wahr et al., 2013), we only used the GNSS vertical displacement observations to retrieve TWS changes in this study. Specifically, the vertical displacement (u) can be represented as the convolution of the mass loading (δm) and the vertical displacement Green's function (F)

$$u(\theta, \lambda, \psi) = F \times \delta m = \frac{\delta m \times R}{M_{\text{earth}}} \sum_{l=0}^{\infty} h_l P_l(\cos \psi) \quad (9)$$

where θ and λ denote the latitude and longitude of the locations of GNSS stations, while ψ represents the angular distance between the GNSS station and the mass loading; M_{earth} (5.965×10^{24} kg) indicates the mass of the Earth; h_l are the loading Love numbers corresponding to vertical displacement provided by H. Wang et al. (2012).

The linear model of Equation 9 can be described as follows:

$$\mathbf{y}_2 = \mathbf{A}_2 \mathbf{x} + \mathbf{e}_2, \quad \mathbf{e}_2 \sim (0, \sigma_{y_2}^2 \mathbf{I}_{y_2}) \quad (10)$$

where $\mathbf{y}_2 = \{u_i\}_{i=1,2,\dots,n_2}$ represents the GNSS vertical displacement vector, n_2 is total number of GNSS stations;

$$\mathbf{A}_2 = \begin{bmatrix} F_{11} & F_{12} & \cdots & F_{1M} \\ F_{21} & F_{22} & \cdots & F_{2M} \\ \vdots & \vdots & \ddots & \vdots \\ F_{n_2 1} & F_{n_2 2} & \cdots & F_{n_2 M} \end{bmatrix} \quad \text{denotes the Green's function coefficient matrix linking } \mathbf{x} \text{ and } \mathbf{y}_2; \mathbf{e}_2 \text{ and } \sigma_{y_2}^2$$

represent the error vector and error variance of the GNSS vertical displacement observations, and \mathbf{I}_{y_2} is the identity matrix corresponding to the length of \mathbf{y}_2 .

In a specific study region (e.g., in Brazil), the number of GNSS stations is always less than the parameters to be estimated and there are correlations between adjacent GNSS stations, both of these will lead to a large condition number for the normal matrix (i.e., $\mathbf{A}_2^T \mathbf{A}_2$). Therefore, the inversion of GNSS vertical displacements for regional TWS changes is an ill-posed problem. In this study, we utilized the frequently used Tikhonov regularization method to stabilize the inversion results. The objective function of the GNSS-only inversion model is as follows:

$$\min \left\{ \left\| \frac{\mathbf{A}_2 \mathbf{x} - \mathbf{y}_2}{\sigma_{y_2}} \right\|^2 + \beta^2 \|\mathbf{Lx}\|^2 \right\} \quad (11)$$

where \mathbf{L} is regularization constraint matrix, which is often expressed as the Laplacian matrix in the GNSS-only inversion model; β^2 is the regularization parameter that controls the strength of constraints. The TWS changes recovered from GNSS-only observations are as follows:

$$\hat{\mathbf{x}} = \left(\mathbf{A}_2^T \mathbf{A}_2 + \sigma_{y_2}^2 \beta^2 \mathbf{L}^T \mathbf{L} \right)^{-1} \mathbf{A}_2^T \mathbf{y}_2 \quad (12)$$

where $\sigma_{y_2}^2 \beta^2$ is determined by the generalized cross validation (GCV) method (Golub et al., 1979) in the present study.

3.3. Joint Inversion Model

Given the complementarity of GRACE and GNSS for retrieving TWS changes in the spatial coverage, spatio-temporal resolution, and spectrum sensitivity, we proposed a new joint inversion model that jointly inverts GRACE L1b data estimated GPD observations and GNSS vertical displacements to obtain reliable TWS changes with high spatio-temporal resolution. Since the normal matrix of the GNSS-only inversion model is more ill-conditioned than the GRACE-only inversion model, the corresponding condition numbers of the normal matrix of GNSS-only and GRACE-only inversion models are 1.3447×10^{22} and 1.2205×10^{21} (considered from the average value of 89 months from January 2008 to July 2016, see Figure S2 in Supporting Information S1), respectively. Hence, we only introduced the Laplacian constraint matrix to stabilize the joint inversion results. The objective function of the joint inversion strategy is as follows:

$$\min \left\{ \left\| \frac{(\mathbf{A}_1 \mathbf{x} - \mathbf{y}_1)}{\sigma_{y_1}} \right\|^2 + \left\| \frac{(\mathbf{A}_2 \mathbf{x} - \mathbf{y}_2)}{\sigma_{y_2}} \right\|^2 + \kappa^2 \|\mathbf{L} \mathbf{x}\|^2 \right\} \quad (13)$$

The joint estimates of TWS change vector derived from GRACE and GNSS observations can be obtained from the joint adjustment method as follows:

$$\hat{\mathbf{x}} = \left(\frac{\mathbf{A}_1^T \mathbf{A}_1}{\sigma_{y_1}^2} + \frac{\mathbf{A}_2^T \mathbf{A}_2}{\sigma_{y_2}^2} + \kappa^2 \mathbf{L}^T \mathbf{L} \right)^{-1} \left(\frac{\mathbf{A}_1^T \mathbf{y}_1}{\sigma_{y_1}^2} + \frac{\mathbf{A}_2^T \mathbf{y}_2}{\sigma_{y_2}^2} \right) \quad (14)$$

where $\frac{1}{\sigma_{y_1}^2}$ and $\frac{1}{\sigma_{y_2}^2}$ represent the relative weights of GRACE and GNSS observations, while κ^2 denotes the regularization parameter. In the inversion of measured data, we attempted to estimate the relative weights and optimal regularization parameter of the joint inversion model using two commonly used methods, one is the VCE method, and the other is ABIC method (Akaike, 1998; Luo et al., 2016). For details of these two methods, please see Text S1 in Supporting Information S1.

3.4. Research Framework

To better visually illustrate our inversion results, the flowchart of this study is shown in Figure 5. The “Checkerboard Test” part examines the spatial resolution of TWS changes derived from 103 GNSS stations in Brazil. The “Closed-loop Simulation” part evaluates the superiority of our new proposed joint inversion model compared to the GRACE-only (GPD-mascon) and GNSS-only models by using the ESM AOHIS SH products. The “Measured Data Inversion and Analysis” part investigates monthly and weekly spatio-temporal evolutions of TWS changes derived from measured GRACE-based GPDs and GNSS vertical displacements based on the GPD-mascon, GNSS, and their joint inversion. Meanwhile, the superiority of the joint inversion model is further assessed through the official GRACE mascon and SH products, independent hydrometeorological data, in situ R time series, and river water level time series.

4. Results and Discussion

4.1. Closed-Loop Simulation

The spatial resolution and reliability of GNSS-inverted TWS changes are related to the number and spatial distribution of GNSS stations, and hence, we first implemented a checkerboard test for examining the spatial

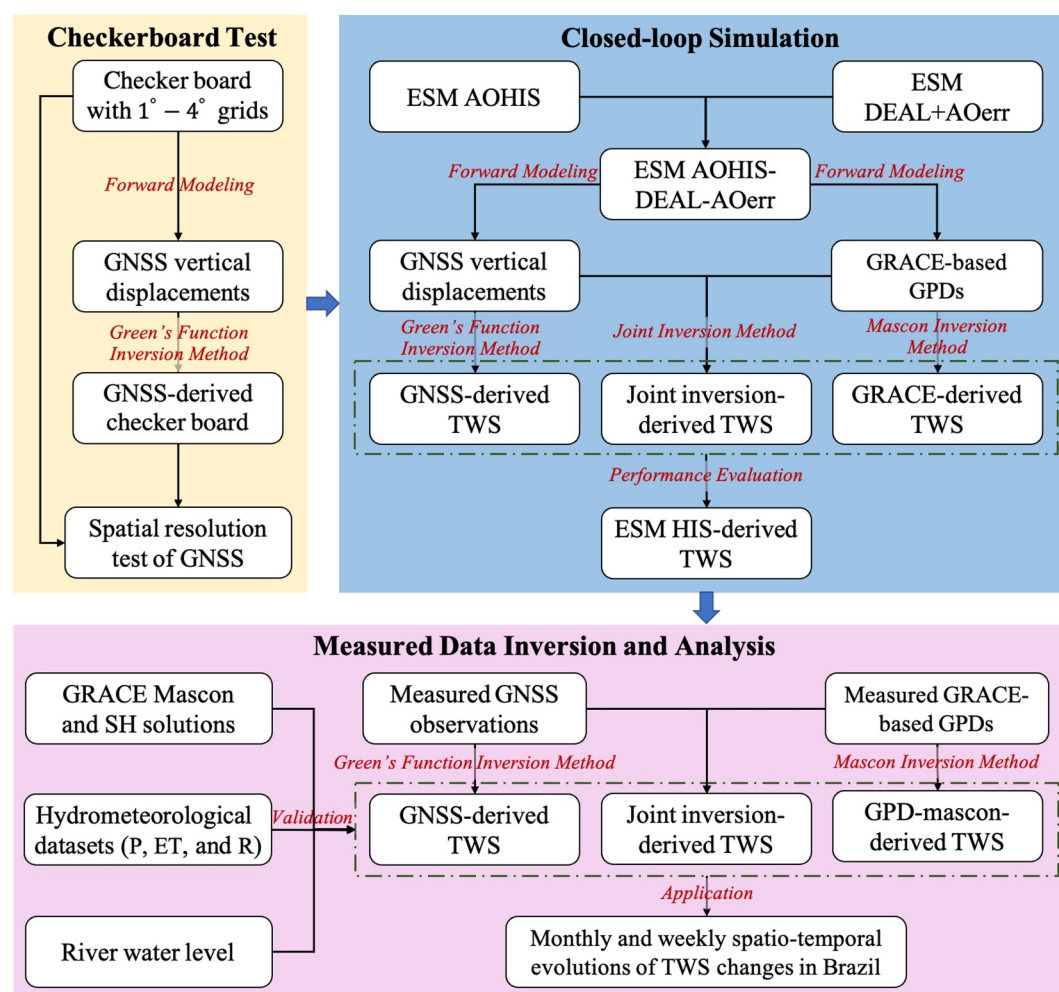


Figure 5. Illustration of the flowchart in this study.

resolution of GNSS-inverted TWS changes in Brazil. The simulation process of the checkerboard test is presented in Figure 5. Figure 6a–6e show the spatial patterns of input checkerboard signals with the spatial resolution of 1°, 2°, 2.5°, 3°, and 4° grids, and the corresponding inversion results are presented in Figure 6f–6j. The white and brown checkerboards represent the 0 and 300 mm EWH signals, respectively. As shown in Figure 6f–6j, the 2.5° and 3° checkerboard signals can be well recovered in southeastern Brazil with dense GNSS stations. However, the GNSS stations are relatively sparsely distributed in northwestern Brazil, the checkerboard signals with the spatial resolution of 3° or even 4° cannot be well recovered. Since the spatial resolution of GRACE solutions is approximately 300 km, it can provide a good complement to GNSS observations in northwestern Brazil. Therefore, the spatial distribution of GRACE and GNSS observations form complementary advantages in Brazil, which provides good support for recovering reliable TWS changes based on the joint inversion of GRACE and GNSS data. To better assess the performance of GRACE and GNSS for retrieving TWS changes in the inversion of measured data, we divided Brazil into northwestern Brazil (light blue region in Figure S4 in Supporting Information S1) and southeastern Brazil (pink region in Figure S4 in Supporting Information S1) according to the spatial distribution of GNSS stations. Table S1 in Supporting Information S1 lists the maximum, minimum, and average distances between the adjacent GNSS stations of the entire Brazil and its northwestern and southeastern regions. As listed in Table S1 in Supporting Information S1, the maximum and minimum distances between the adjacent GNSS stations are 593.38 and 0.01 km in entire Brazil, 593.38 and 1.6 km for northwestern Brazil, and 436.15 and 0.01 km for southeastern Brazil. Meanwhile, the average distances of GNSS stations in Brazil and its northwestern and southeastern regions are 309.39, 415.32, and 240.77 km, respectively. This indicates that the spatial resolution of TWS changes retrieved by GRACE and GNSS is comparable for the entire Brazil.

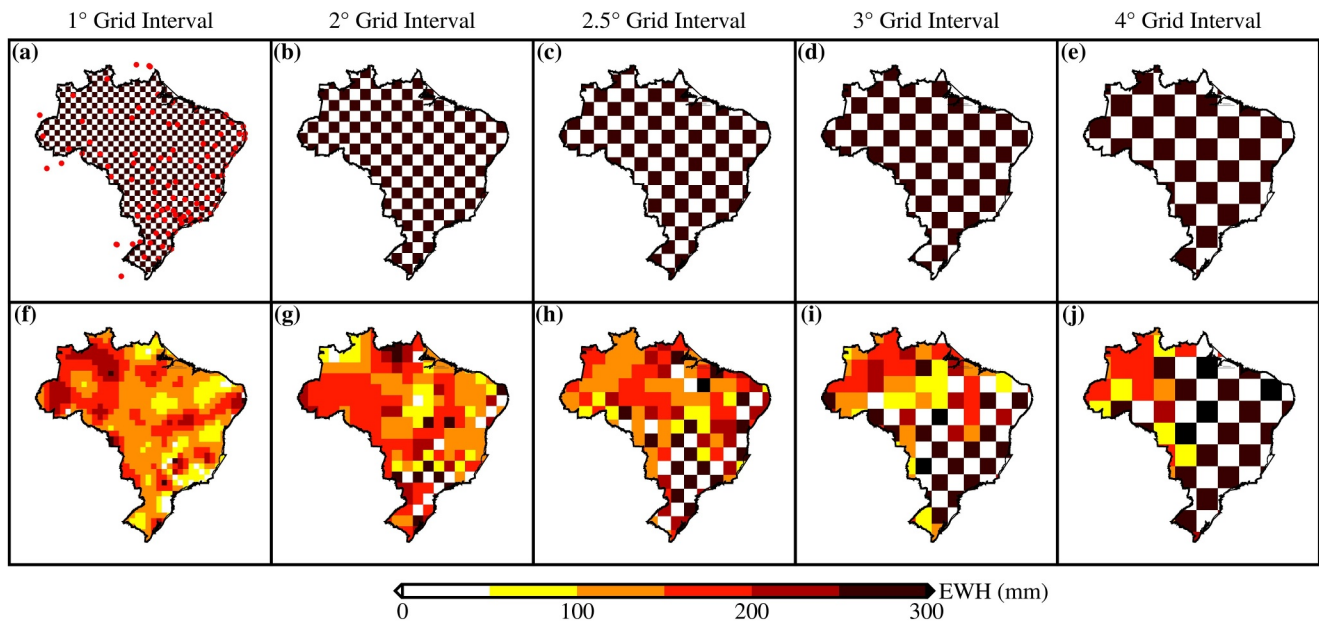


Figure 6. Spatial resolution test of 103 GNSS stations in Brazil using the checkerboard grids: (a)–(e) represent the input checkerboard signals with the spatial resolution of 1°, 2°, 2.5°, 3°, and 4° grids, respectively, (f)–(j) indicate the corresponding GNSS-only inversion results. The red dots in (a) indicate the locations of GNSS stations.

As there are no true TWS changes for evaluating the performance of TWS changes derived from measured GRACE, GNSS, and their joint inversion, we initially utilized the AOHIS SH products from January 2004 to December 2006 for closed-loop simulation evaluation. First, the TWS changes derived from the ESM HIS SH products were used as the “true” signals. Second, the differences between the ESM AOHIS and DEAL+Aoerr SH products were used to simulate the GRACE-based GPD observations and GNSS vertical displacements. To be consistent with measured GRACE and GNSS observations, the Gaussian white noises with standard deviations of $0.001 \text{ m}^2/\text{s}^2$ (Zhong et al., 2020) and 3 mm (S. Wang et al., 2022) were added to the simulated GPD observations and GNSS vertical displacements, respectively. Third, the TWS changes derived from simulated GPD observations and GNSS vertical displacements and their joint inversion were utilized to compare with the “true” signals for performance evaluation. It is noteworthy that since the “true” TWS changes are known in the closed-loop simulation, we determined the optimal regularization parameters of the three inversion models by minimizing the root mean square error (RMSE) between the inversion results and “true” signals. The flowchart of the closed-loop simulation is presented in Figure 5.

Figure 7 shows spatial patterns of “true” TWS changes from degree-60 HIS SH solutions (input signals), the TWS changes derived from three inversion models (GPD-mascon, GNSS, and joint inversion), and the corresponding residuals between different inversion results and input signals in January 2006. As shown in Figure 7, the patterns of TWS change from these three inversion models present good consistency with the input signals, while the signal amplitudes of GNSS estimates are weaker than those from GPD-mascon and joint inversion solutions. In addition, the signal amplitudes of residuals from joint inversion are smaller than those from GPD-mascon and GNSS results, and the spatial CCs and STDs between the input signals and the three inverted results (i.e., GPD-mascon, GNSS, and joint inversion) are 0.94 and 51.75 mm, 0.78 and 93.36 mm, and 0.96 and 41.03 mm, respectively. It demonstrates that the TWS changes derived from our joint inversion strategy show better stability and reliability than those from the GPD-mascon and GNSS results. In addition to the degree-60 HIS SH solutions, we also used the degree-100 and degree-180 HIS SH solutions for analysis (Figure S5 in Supporting Information S1). As shown in Figure S5 in Supporting Information S1, although the input signals from degree-100 and degree-180 HIS SH solutions present more spatial details compared to the degree-60 HIS, the inverted TWS changes from these three inversion models are still similar to those of degree-60 HIS owing to the limited spatial resolution ($\sim 300 \text{ km}$) of GRACE and GNSS in Brazil. Meanwhile, the joint inversion still presents better performance than those of GPD-mascon and GNSS solutions. For this reason, we only used the degree-60 HIS SH solutions for closed-loop simulation in this work. Additionally, we also investigated the performance of the joint

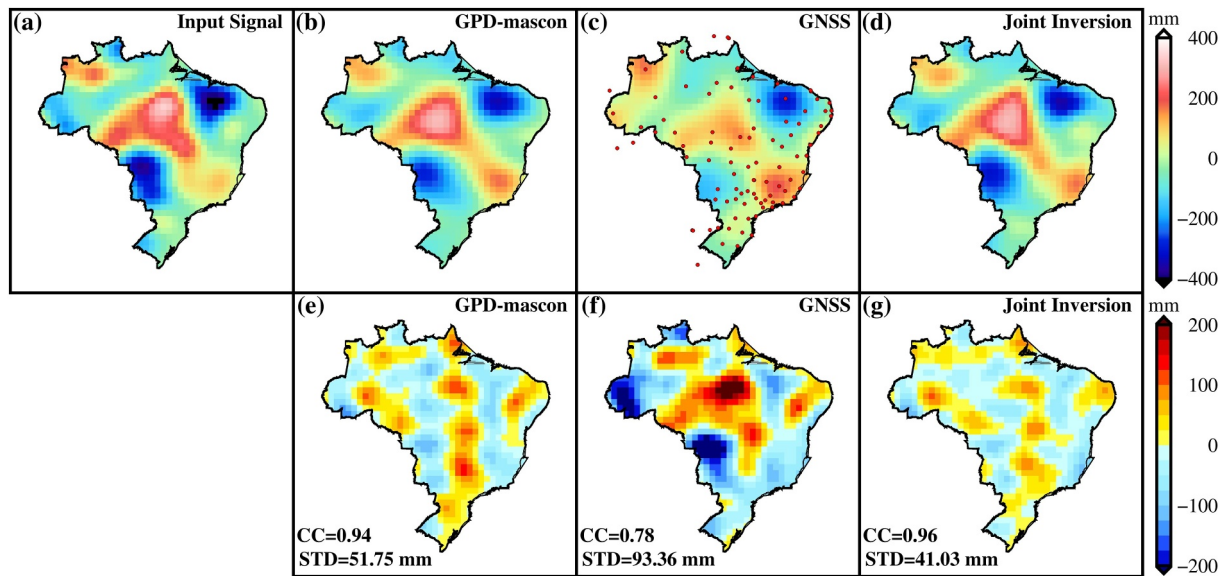


Figure 7. Comparison of the input signals (a) from degree-60 HIS spherical harmonic (SH) coefficients, inverted TWS changes from (b) GPD-mascon, (c) GNSS, and (d) joint inversion in January 2006, and (e)–(g) present the corresponding residuals between the input signals and inversion results.

inversion model in recovering TWS changes with higher spatial resolution (i.e., better than 300 km; see Text S3 and Figure S6 through Figure S8 and Table S2 in Supporting Information S1), the results demonstrate that our joint inversion model can recover TWS changes with higher spatial resolution when sufficient GNSS observations are available.

To further assess the superiority of the joint inversion model over the GRACE- and GNSS-only inversion models, we compared the TWS change time series from the input signals and the three inversion models and corresponding CCs and STDs from January 2004 to December 2006, and investigated the impacts of different GNSS noise levels (1, 2, and 3 mm for vertical displacements) on the recovery of TWS changes (Figure 8). As shown in Figures 8a–8c, the TWS change time series from these three inversion strategies generally present good consistency with input signals, but the signal amplitudes of GNSS estimates are larger than other results. This is because the ground-based GNSS observation is more sensitive to local water loading than satellite-based GRACE observation. In addition, the joint inversion results show better consistency (lower STDs and higher correlations) with the input signals compared to the GPD-mascon and GNSS solutions when the GNSS vertical displacements with 1 mm, 2 mm, and 3 mm noise levels (Figures 8d–8f). Among them, the mean STDs and CCs are 45.48 mm and 0.95 for GPD-mascon, 88.05 mm and 0.81 for GNSS (with a 3 mm noise level), and 42.02 mm and 0.96 for joint inversion during 2004–2006, respectively. In addition, when the accuracy of GNSS vertical displacements increases to 1 mm, the mean STDs and CCs of GNSS and joint results are 64.19 mm and 0.91 versus 35.74 mm and 0.97, respectively. It demonstrates that our proposed joint inversion model presents better performance than GPD-mascon and GNSS with a 3 mm noise level (the current precision level of GNSS vertical displacements), the corresponding STDs compared to GPD-mascon and GNSS solutions decrease by 2.5 and 42.5 mm, and correlations increase by 1% and 15%. When the accuracy of GNSS vertical displacements increases to 1 mm, the STDs of joint inversion decrease by 10 and 28.5 mm compared to GPD-mascon and GNSS solutions, and the corresponding correlations increase by 2% and 5%, respectively.

Figure 9 shows the patterns of STDs of residuals between the inverted TWS changes from the three inversion models and input signals at each grid cell. It shows that the STDs of GNSS inversion results (especially in Northwestern Brazil with relatively sparse GNSS stations) are significantly larger than those of GPD-mascon and joint inversion results. The patterns of joint inversion are generally close to GPD-mascon, while the amplitudes are weaker, especially in southeastern Brazil with relatively dense GNSS stations. The mean STDs of joint inversion results decrease by ~6.98 and ~37.5 mm compared to GPD-mascon and GNSS (with a 3 mm noise level) solutions, respectively, and the corresponding values are ~8.5 and ~30.66 mm when GNSS with a 2 mm noise level, and ~12.82 and ~21.83 mm when GNSS with a 1 mm noise level, respectively. We observe that, with

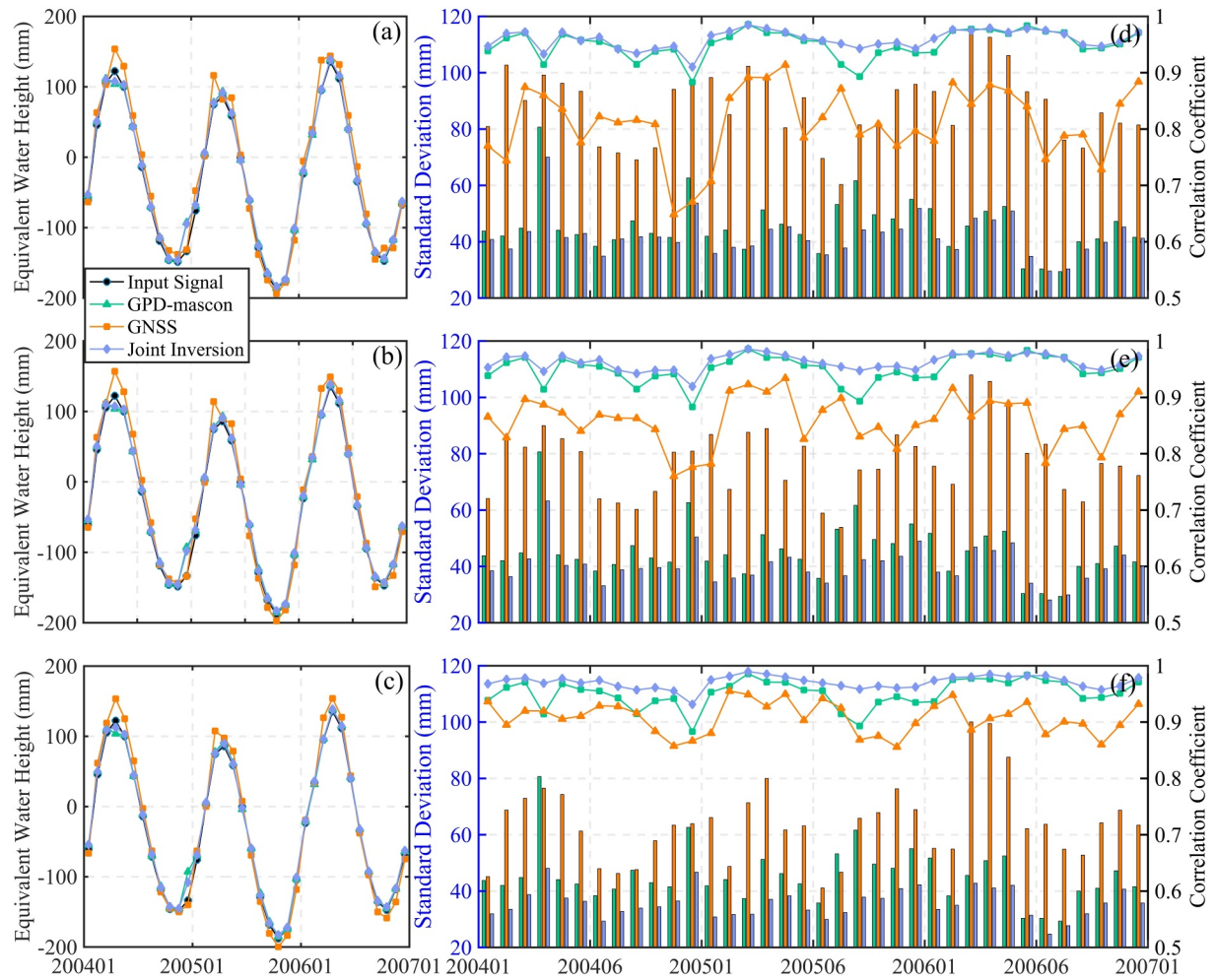


Figure 8. (a) Time series of HIS-derived TWS change and the inversion results from simulated GRACE-based GPD observations (with $0.001 \text{ m}^2/\text{s}^2$ noise level), simulated GNSS vertical displacements (with 3 mm noise level), and their joint inversion during 2004–2006; (d) the values of standard deviation (STD) of residuals and correlation coefficient (CC) between the input signals and inversion results, note that the left y-axis is for STDs (histogram) and the right y-axis is for CCs (line chart). Panels (b) and (e), (c) and (f) are the same as (a) and (d) but the GNSS vertical displacements with noise levels of 2 and 1 mm, respectively. Note that the noise level of GRACE-based GPDs remains unchanged in the joint inversion model.

the improvement of GNSS observation accuracy, the superiority of joint inversion over the GPD-mascon and GNSS will be significantly improved. In general, the TWS changes derived from joint inversion are more reliable and accurate than those from GRACE-only (GPD-mascon) and GNSS-only solutions in the spatio-temporal domains.

4.2. Spatio-Temporal Changes in TWS Over Brazil

We estimated the monthly and weekly TWS changes in Brazil spanning the period from January 2008 to July 2016 using measured GRACE-based GPD observations and GNSS vertical displacements and their combination. Since there are no “true” TWS changes that can be used as references for determining optimal regularization parameters based on the RMSE criterion in the inversion of measured data. The regularization parameters of the GRACE-only and GNSS-only inversion models can be effectively determined by the VCE and GCV methods, respectively. For the joint inversion model, we attempted to use two commonly used weighting methods (i.e., VCE and ABIC) to determine the relative weights between GRACE and GNSS data and the regularization parameter of the Laplacian constraint in Equation 14. Figure S9 in Supporting Information S1 reveals the iterative convergence curve of VCE for the joint inversion model in January 2008, as well as the monthly and weekly relative weight ratios between GRACE-based GPD observations and GNSS vertical displacements and the

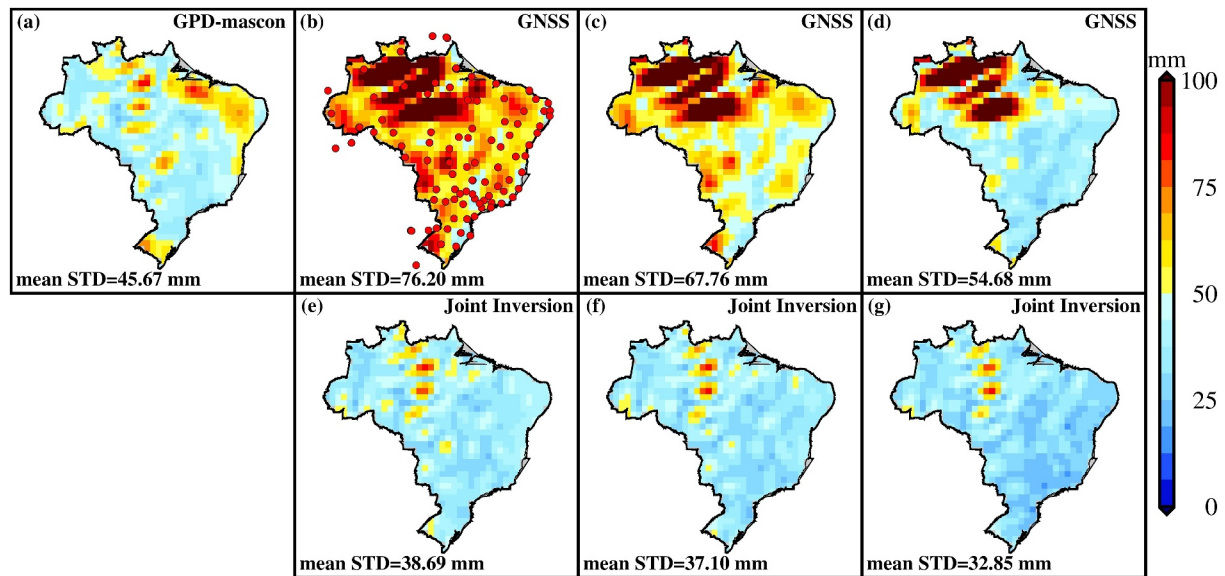


Figure 9. Patterns of standard deviation (STD) of residuals between the input signals (ESM HIS-derived TWS changes) and inversion results from (a) GPD-mascon (GPDs with $0.001 \text{ m}^2/\text{s}^2$ noise level), (b)–(d) GNSS vertical displacements with 3, 2, and 1 mm noise levels, and (e)–(g) correspond to joint inversion. Note that the noise level of GRACE-based GPDs remains unchanged in the joint inversion model, while the noise levels of GNSS vertical displacements in the joint inversion model in (e)–(g) correspond to those in (b)–(d), respectively.

regularization parameters from January 2008 to July 2016. It seems that the VCE slightly overfits the GPD observations in the joint model, and the average relative weight ratios between the GPD observations and GNSS vertical displacements are 4.64 (monthly solutions) and 5.16 (weekly solutions), respectively. Meanwhile, the average regularization parameters of the joint inversion model from VCE for the monthly and weekly solutions are 10.93 and 19.31, respectively. Figure S10 in Supporting Information S1 displays the values of ABIC function in January 2008, as well as the monthly and weekly relative weight ratios between GRACE-based GPD observations and GNSS vertical displacements and the regularization parameters. We observe that the ABIC severely overfits the GNSS vertical displacements, and the average relative weight ratio between GNSS vertical displacements and the GPD observations is approximately 10,000 and the average regularization parameters for monthly and weekly solutions are approximately 1.40×10^{-18} and 6.74×10^{-16} , respectively. Therefore, the traditional VCE and ABIC methods were not applied to the joint inversion model in this work. Nevertheless, given that the spatial resolution of GRACE- and GNSS-derived TWS changes in Brazil is comparable (~ 300 vs. ~ 309 km, see Figure 6 and Table S1 in Supporting Information S1), the relative contributions of measured GRACE and GNSS observations in the joint inversion model are set to equal weights, which is also consistent with the relative weights of GNSS and GRACE data for recovering short-term signals in the joint inversion model of Carlson et al. (2022). In addition, although the VCE has a slight overfitting of GRACE observations, we believe that the regularization parameters determined by the VCE are reasonable than ABIC. Therefore, we used the modified VCE method to determine the regularization parameters for the joint inversion model in the following work.

We compared the monthly TWS changes estimated from the measured GRACE-based GPD observations, GNSS vertical displacements, and their joint inversion with three official (CSR, JPL, and GSFC) mascon solutions in the spatio-temporal domains. Notably, because GIA effects are included in the GNSS vertical displacements and GRACE GPDs, we have applied GIA corrections to the monthly and weekly TWS changes from GNSS, GPD-mascon, and joint inversion using ICE-6G_D model. Figure 10 displays the spatial patterns of annual amplitudes and phases of TWS changes determined from these six solutions (named sequentially as GPD-mascon, GNSS, joint inversion, CSR-M, JPL-M, and GSFC-M). As shown in Figure 10, the patterns of annual amplitudes from these solutions generally present good consistency with each other, and there are significantly strong signal amplitudes in the Amazon basin. We calculated the mean annual amplitudes derived from different solutions over the overlap zone between the Amazon basin and Brazil (red curve in Figure 10a), the mean annual amplitudes of JPL-M (330.37 ± 26.57 mm) and GSFC-M (328.04 ± 26.00 mm) are close and stronger than other solutions,

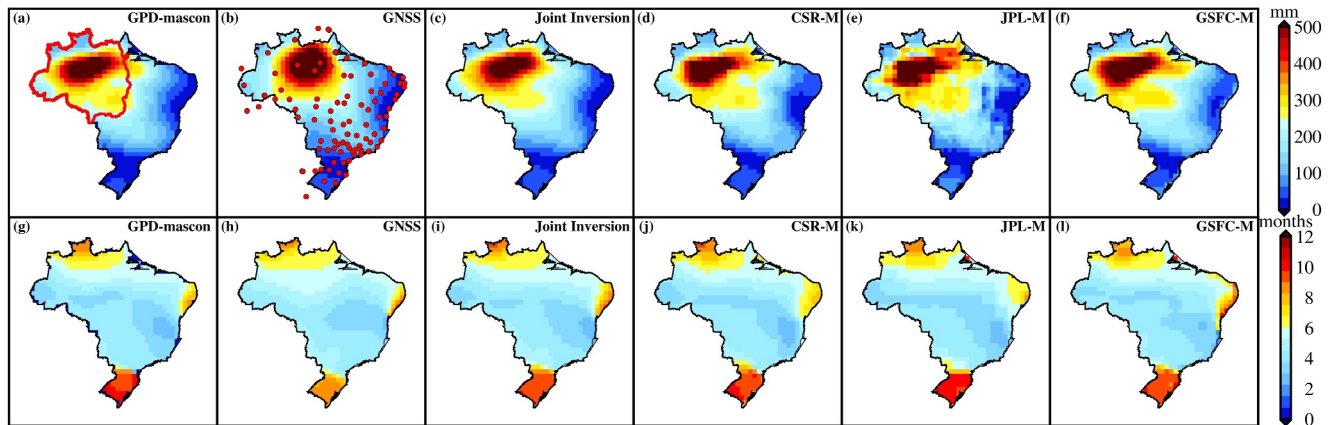


Figure 10. Spatial patterns of annual amplitudes (a–f) and phases (g–l) of the monthly TWS changes derived from the solutions of GPD-mascon, GNSS, joint inversion, and three official mascon products (CSR-M, JPL-M, and GSFC-M) from January 2008 to July 2016. The red curve in (a) indicates the boundary of the overlap zone between the Amazon basin and Brazil, and the red dots in (b) represent the locations of GNSS stations.

followed by the GNSS (323.79 ± 29.24 mm), and then the CSR-M (318.92 ± 34.06 mm), the joint inversion (315.25 ± 30.99 mm) and GPD-mascon (314.20 ± 33.16 mm) are close and the smallest. Note that the uncertainties of the annual amplitude, phase, and long-term trend of TWS changes are all derived from the least squares fitting errors in this study. The patterns of annual phases derived from these six solutions still show good consistency with each other, while the phases of GNSS solutions in southern Brazil lead other GRACE mascon solutions and joint inversion. These differences in amplitude and phase arise from variations in data sources (e.g., satellite-based GRACE observations vs. ground-based GNSS vertical displacements) and data processing strategies (e.g., dynamic approach for official mascon solutions vs. energy balance approach for GPD-mascon solutions) employed by these inversion models.

Figure 11 compares the monthly time series of TWS changes from these six solutions in the entire Brazil and its northwestern and southeastern regions from January 2008 to July 2016. All of these six solutions present significant seasonality and show good consistency with each other in Brazil and its sub-regions. The annual amplitudes and phases and long-term trends of TWS change time series from January 2008 to July 2016 are given in Table 1. For entire Brazil, the amplitude of GSFC-M (176.32 ± 13.18 mm) surpasses than those of other solutions, followed by the amplitude of GNSS solutions (173.89 ± 13.12 mm) which is comparable to JPL-M (174.67 ± 13.31 mm), and then the GPD-mascon (170.11 ± 12.47 mm) with amplitude closes to CSR-M (170.43 ± 12.62 mm), while the joint inversion (168.51 ± 12.44 mm) exhibits the smallest amplitude. The phase obtained from joint inversion (4.79 ± 0.14 months) is closer to the three official mascon solutions (4.76 ± 0.14 , 4.75 ± 0.14 , and 4.77 ± 0.14 months) compared to GNSS (5.12 ± 0.14 months) and GPD-mascon (4.70 ± 0.13 months). In addition, all solutions reveal a declining trend in TWS changes in Brazil during the study period. Among them, the trends of the three official mascon solutions (-10.71 ± 3.57 , -11.66 ± 3.73 , and -12.10 ± 3.77 mm/yr) are closely aligned and the most significant. Following are the GPD-mascon solutions (-9.72 ± 3.53 mm/yr), and the trend of GNSS estimates (-8.98 ± 3.74 mm/yr) is slightly smaller than that of GPD-mascon results. While the trend of joint inversion results (-9.41 ± 3.52 mm/yr) falls between GPD-mascon and GNSS solutions. In northwestern Brazil, GNSS exhibits amplitudes that are closer to JPL-M and GSFC-M, while the amplitudes of GPD-mascon and joint inversion align more closely with CSR-M. The phases obtained from GPD-mascon, joint inversion, and the three official mascon solutions are more consistent and lead the GNSS solutions by approximately 0.33 months. Moving to southeastern Brazil, the amplitudes of GNSS and GPD-mascon solutions are comparable to GSFC-M, and the amplitude of joint inversion results is more consistent with CSR-M and JPL-M solutions. The phase differences among the six solutions are relatively small, with the maximum disparity being less than 0.2 months. Additionally, the relative relationships of long-term trend changes estimated from these six solutions in northwestern and southeastern Brazil are consistent with those of the entire Brazil.

Due to the challenge of acquiring reliable information for assessing the accuracy of individual TWS change products, we utilized the generalized three-cornered hat (GTCH) method (Chen et al., 2021; Long et al., 2014;

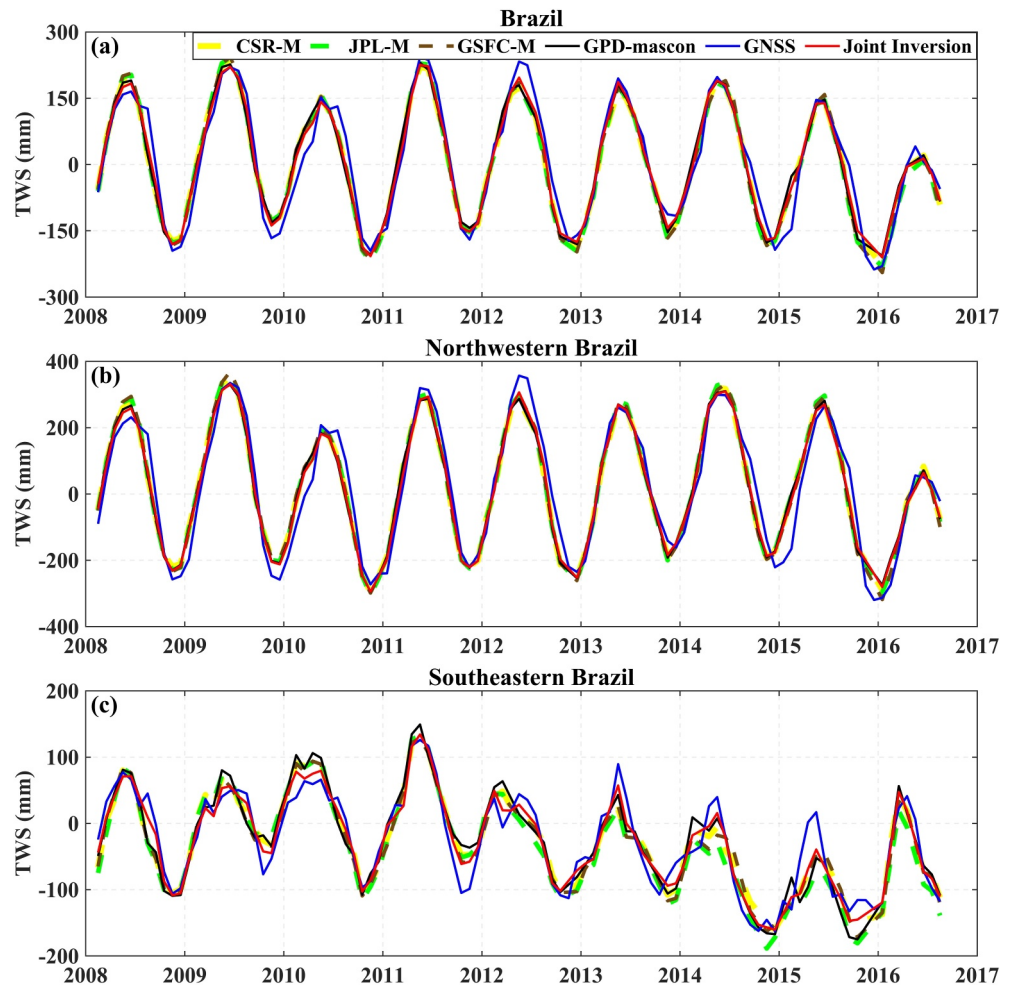


Figure 11. Monthly TWS change time series derived from the solutions of GPD-mascon, GNSS, joint inversion, and three official mascon solutions (CSR-M, JPL-M, and GSFC-M) in (a) Brazil and its (b) northwestern and (c) southeastern regions from January 2008 to July 2016.

Premoli & Tavella, 1993) to roughly evaluate the uncertainties of TWS change time series determined from these six solutions in Brazil and its northwestern and southeastern regions (Table 2). The specific calculation method for estimating the uncertainty of TWS changes using the GTCH method is presented in Text S2 in Supporting Information S1. As indicated by Table 2, the uncertainties of GNSS solutions are considerably larger than those of other solutions due to relatively large observation errors. The uncertainty of GNSS estimates in northwestern Brazil (51.94 mm), attributed to the sparsely distributed GNSS stations, is significantly larger than that in southeastern Brazil (28.12 mm). Additionally, for the entire Brazil, CSR-M exhibits the lowest uncertainty (5.05 mm), followed by our joint inversion (6.77 mm). Subsequently, the uncertainty of GPD-mascon (8.89 mm) is comparable to JPL-M (8.90 mm) and GSFC-M (8.89 mm) solutions. In northwestern Brazil, our joint inversion results show the smallest uncertainty (6.61 mm) than other solutions. In southeastern Brazil, the accuracy of the joint inversion results (9.43 mm) is slightly lower compared to CSR-M (6.60 mm) and GSFC-M (8.42 mm) solutions, however, it is still better than GPD-mascon (11.41 mm) and JPL-M (14.32 mm) solutions, and significantly better than GNSS results (28.12 mm). It demonstrates that the joint inversion model provides a more stable and reliable estimation of TWS changes across Brazil and its two sub-regions compared to GNSS and GPD-mascon solutions through the analysis of the GTCH method.

Due to the relatively sparse data coverage of GRACE over short temporal scales (e.g., daily and weekly), most of the GRACE SH and mascon products have temporal resolution of one month. Although GNSS can provide daily vertical displacement time series, the uncertainty in these daily time series is relatively large. Therefore, this study

Table 1

Annual Amplitudes and Phases, and Long-Term Trends of Monthly TWS Change Time Series Derived From the Solutions of GNSS, GPD-Mascon, Joint Inversion, and Three Official Mascon Solutions (CSR-M, JPL-M, and GSFC-M) in Brazil and Its Northwestern and Southeastern Regions

Region	Solutions	Amplitude (mm)	Phase (months)	Trend (mm/yr)
Brazil	GNSS	173.89 ± 13.12	5.12 ± 0.14	-8.98 ± 3.74
	GPD-mascon	170.11 ± 12.47	4.70 ± 0.13	-9.72 ± 3.53
	Joint Inversion	168.51 ± 12.44	4.79 ± 0.14	-9.41 ± 3.52
	CSR-M	170.43 ± 12.62	4.76 ± 0.14	-10.71 ± 3.57
	JPL-M	174.67 ± 13.31	4.75 ± 0.14	-12.10 ± 3.77
	GSFC-M	176.32 ± 13.18	4.77 ± 0.14	-11.66 ± 3.73
Northwestern Brazil	GNSS	251.95 ± 20.48	5.31 ± 0.15	-6.21 ± 5.84
	GPD-mascon	243.50 ± 19.76	4.85 ± 0.15	-6.55 ± 5.59
	Joint Inversion	242.48 ± 20.02	4.91 ± 0.15	-6.51 ± 5.66
	CSR-M	244.73 ± 19.91	4.89 ± 0.15	-8.52 ± 5.63
	JPL-M	252.12 ± 20.86	4.89 ± 0.15	-8.68 ± 5.90
	GSFC-M	252.09 ± 20.77	4.89 ± 0.15	-9.95 ± 5.88
Southeastern Brazil	GNSS	71.92 ± 9.91	4.09 ± 0.27	-13.06 ± 2.83
	GPD-mascon	70.00 ± 13.16	3.91 ± 0.36	-14.38 ± 3.74
	Joint Inversion	65.41 ± 11.58	4.09 ± 0.34	-13.68 ± 3.29
	CSR-M	65.51 ± 12.08	4.06 ± 0.35	-13.95 ± 3.43
	JPL-M	66.21 ± 13.17	3.98 ± 0.38	-17.18 ± 3.74
	GSFC-M	69.22 ± 11.58	4.08 ± 0.32	-14.19 ± 3.29

Note. The uncertainty represents the least squares fitting error.

employs a joint inversion model and utilizes Laplacian constraint to integrate the respective advantages of GNSS and GRACE in both temporal and spatial scales. This allows for the estimation of weekly TWS change time series in Brazil. Figure 12 illustrates the spatial evolutions of TWS changes from our three inversion models (i.e., GNSS, GPD-mascon, and joint inversion) and the GFZ weekly SH solutions in Brazil during the first 5 weeks of 2009. It is noteworthy that, to preserve more hydrological signals, we only used a 300 km Gaussian filtering to smooth the GFZ weekly SH solutions. As illustrated in Figure 12, the TWS changes determined by these solutions all exhibit alternating positive and negative anomaly signals in Brazil. Among them, the signal amplitudes and patterns of GNSS estimates exhibit some differences compared to other solutions owing to the differences in the spatial distribution and spectral sensitivity of these two observation technologies. The spatial patterns of the joint inversion results fall between the GPD-mascon and GNSS solutions. Between the two GRACE-only solutions (GPD-mascon vs. GFZ-SH), GPD-mascon benefits from regularization constraints, resulting in stronger signal amplitudes and presenting more spatial details. In general, our weekly solutions maintain good consistency with the GFZ SH solution. However, there are still some differences in terms of signal strength and spatial details due to the differences in data sources and data processing strategies.

Figure 13 shows the weekly TWS change time series determined from our three inversion models (GPD-mascon, GNSS, and joint inversion) and GFZ SH solutions, and the monthly joint inversion results are also used for

Table 2

The Uncertainty (Unit: mm) of the Monthly TWS Change Time Series Derived From the Six Solutions Estimated by the Generalized Three-Cornered Hat (GTCH) Method in Brazil and Its Northwestern and Southeastern Regions From January 2008 to July 2016

Region	GNSS	GPD-mascon	Joint inversion	JPL-M	CSR-M	GSFC-M
Brazil	34.71	8.89	6.77	8.90	5.05	8.89
Northwestern Brazil	51.94	8.56	6.61	9.09	6.86	11.18
Southeastern Brazil	28.12	11.41	9.43	14.32	6.60	8.42

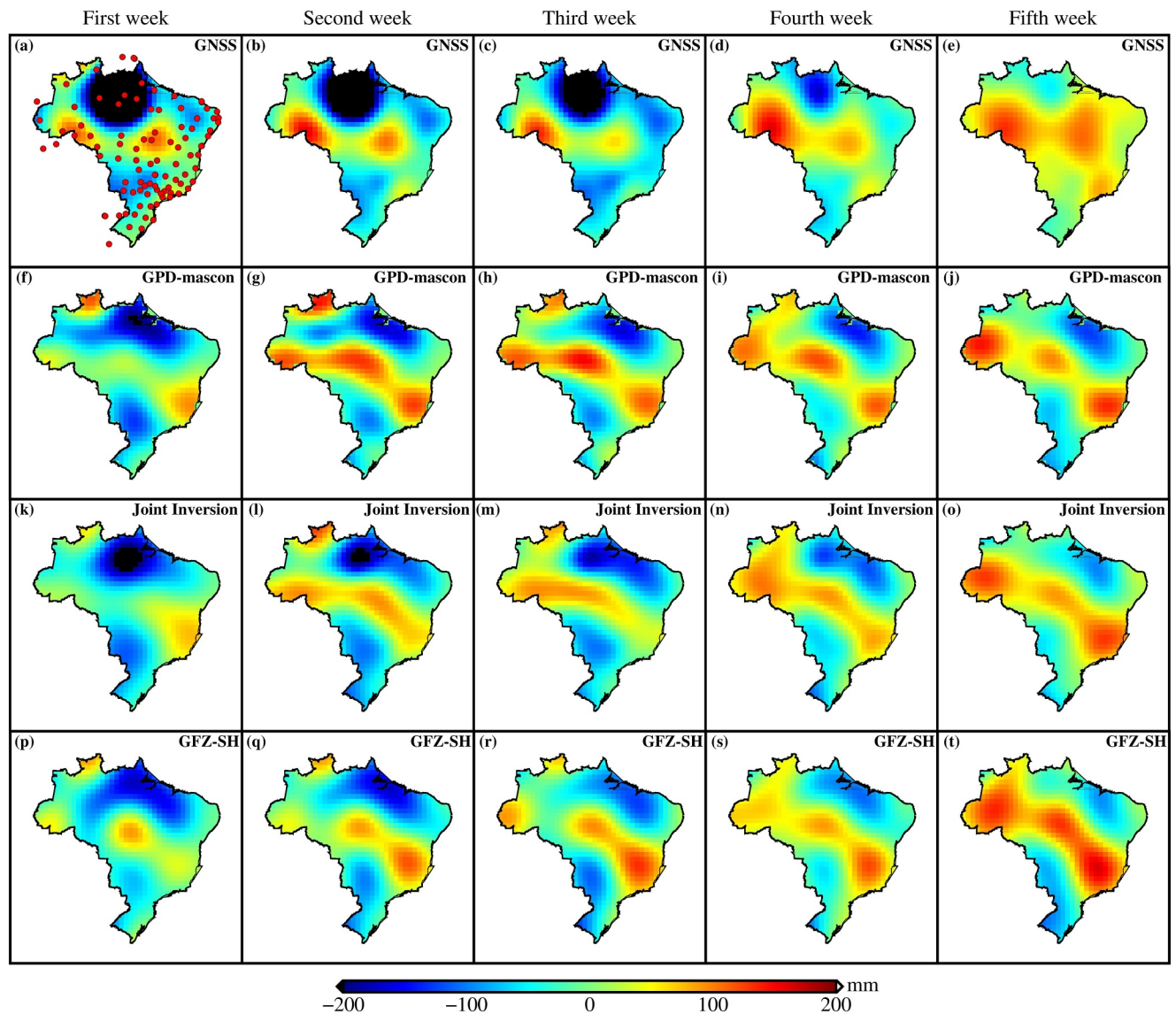


Figure 12. Spatial evolutions of weekly TWS changes derived from (a–e) GNSS, (f–j) GPD-mascon, (k–o) joint inversion, and (p–t) GFZ spherical harmonic (SH) solutions in the first 5 weeks of 2009. The red dots present the locations of GNSS stations.

comparison. Note that the weekly GFZ SH solutions are available only up to February 2013. As shown in Figure 13, the weekly TWS change time series display more high-frequency information than the monthly solutions in Figure 11. In northwestern Brazil, the joint inversion results are more consistent with GPD-mascon solutions ($CC = 0.99$ and $STD = 26.51$ mm) than GNSS solutions ($CC = 0.96$ and $STD = 52.32$ mm) due to the relatively sparsely distributed GNSS stations. But the opposite is true in southeastern Brazil with a relatively dense distribution of GNSS stations, the CC and STD between joint inversion and GPD-mascon are 0.92 and 27.69 mm, while the corresponding values between joint inversion and GNSS are 0.98 and 15.35 mm. It shows that the spatial coverage of GRACE and GNSS data complement each other, which provides good support for the joint inversion of GRACE and GNSS data to obtain reliable TWS changes.

Comparing our three inversion results, the TWS changes estimated by the GFZ SH solutions present a systematic bias in the entire Brazil and northwestern Brazil between August 2012 to February 2013 (first gray area in Figure 13). This could be attributed to post-processing of the GRACE SH coefficients (e.g., Gaussian filtering). Additionally, there are significant anomalies of GPD-mascon and jointly inverted TWS changes in Brazil and northwestern Brazil in November 2015 (second gray area in Figure 13), which is attributed to the inadequacy of

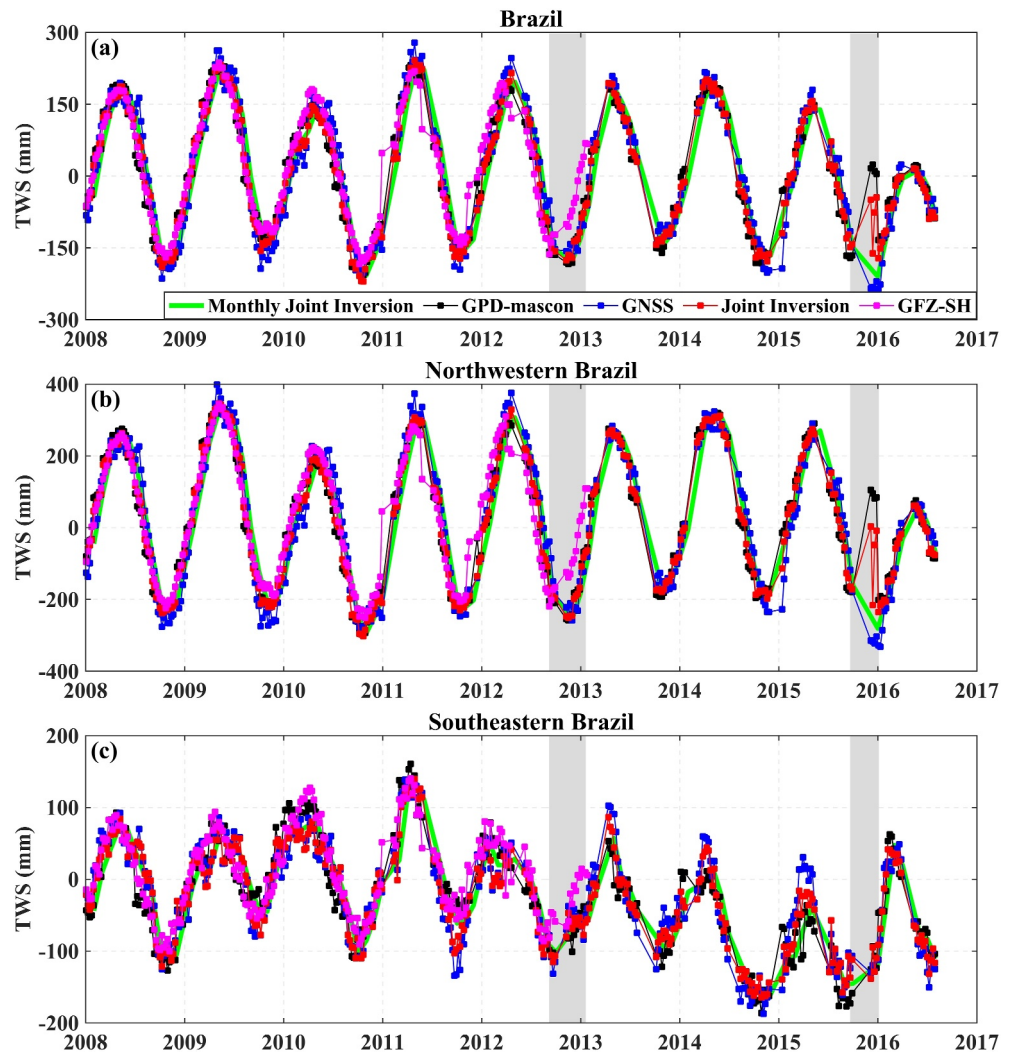


Figure 13. Weekly TWS change time series derived from GPD-mascon, GNSS, joint inversion (from January 2008 to July 2016), and GFZ spherical harmonic (SH) solutions (from January 2008 to February 2013) in (a) Brazil and its (b) northwestern and (c) southeastern regions from January 2008 to July 2016, with the monthly joint inversion results are used for comparison.

weekly GRACE GPD observations (see Figure S11 in Supporting Information S1). However, the weekly GNSS estimates maintain good consistency with the monthly joint inversion results, indicating that GNSS can serve as a good supplement for the GRACE observations with poor data quality and missing data, as well as the data gap between the GRACE and GRACE-FO missions.

4.3. Performance Evaluation of the Joint Inversion Results

In Section 4.1, we have validated the performance of the joint inversion model through closed-loop simulations. This section further assesses the effectiveness and reliability of the joint inversion results over the GRACE-only and GNSS-only solutions using external independent observational data. Within specific watersheds and regional scopes, the TWS changes can be approximately expressed using P, ET, and R based on the water budget closure method. We converted monthly P and ET (from ERA5, GLDAS, and WGHM outputs) and dS_t/dt time series (from GPD-mascon, GNSS, and joint inversion results) into R variations using the water budget closure method ($P-ET-dS_t/dt$), and compared them with in situ R time series at the Obidos hydrological station (Figure 14). It is noteworthy that we employed the GTCH method (see Text S3 in Supporting Information S1) to fuse these three data products to obtain more reliable P and ET time series for reducing the discrepancies between different data products. As shown in Figure 14, the R time series derived from model-simulated P and ET, as well as TWS

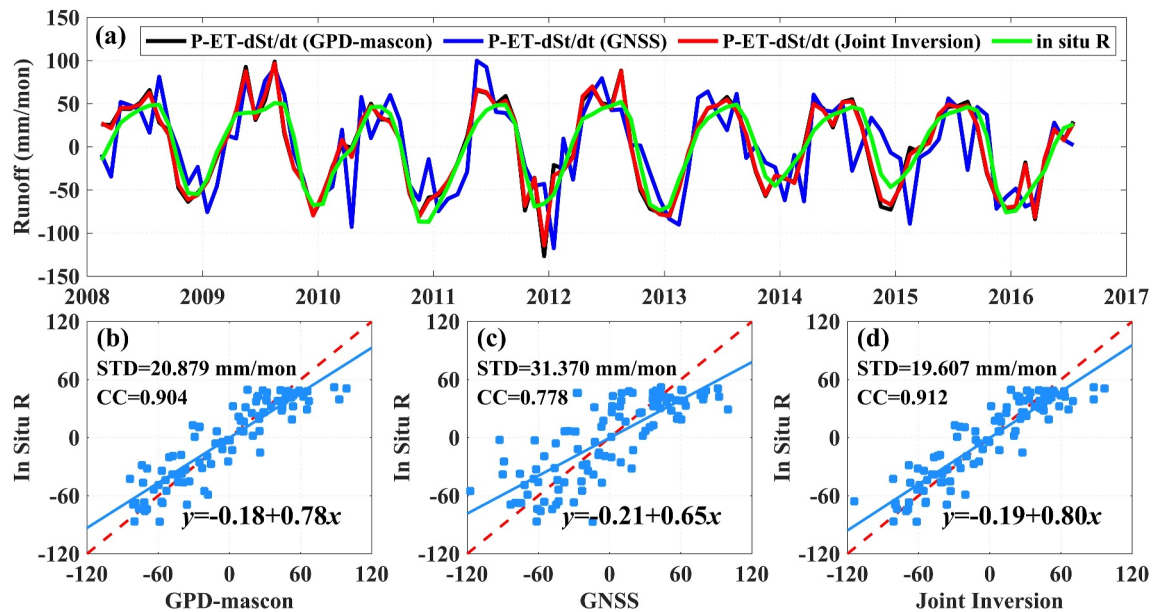


Figure 14. (a) Monthly runoff (R) time series derived from GTCH-fused precipitation (P) and evapotranspiration (ET), and dS_t/dt from three inversion solutions (GPD-mascon, GNSS, and joint inversion) based on water budget closure and in situ R measurements from January 2008 to July 2016, (b–d) present the scatter plots depicting the in situ R measurements in comparison with the results of GPD-mascon, GNSS, and joint inversion, respectively.

changes from different satellite geodetic inversion results, demonstrate excellent consistency with the in situ R time series. Table S3 in Supporting Information S1 lists the STDs and CCs between the simulated R time series from different data sources and the in situ R time series. The joint inversion results show the highest consistency with the in situ R time series than those from the GPD-mascon and GNSS inversion results, and the corresponding STDs and CCs (considered from GTCH-fused $P-ET$ minus dS_t/dt) are 19.607 mm and 0.912, 20.879 mm and 0.904, and 31.370 mm and 0.778, respectively. This comparison highlights that the joint inversion can effectively synthesize the respective advantages of GRACE and GNSS observations, leading to a more stable and reliable TWS change time series.

Figure 15 provides the CC statistics between the monthly TWS change time series estimated by the three inversion methods (GPD-mascon, GNSS, and joint inversion) and the monthly river water level time series from 162 “virtual” gauge stations observed by satellite altimetry. It can be observed that the overall correlations for GPD-mascon and joint inversion results are higher than those of the GNSS estimates, which is because the majority of “virtual” stations are distributed in northwestern Brazil, where the GNSS stations are sparsely distributed. When the CC of GNSS solutions is greater than 0.4 (for a total of 100 virtual stations), the average CC of the joint results (0.732) at these 100 stations is higher than those of GNSS (0.649) and GPD-mascon (0.727) solutions. Furthermore, when the CC of GNSS solutions exceeds 0.5 (for a total of 79 virtual stations), the average CCs for joint inversion, GNSS, and GPD-mascon solutions at these 79 stations are 0.778, 0.702, and 0.767, respectively, further validating the reliability of the monthly joint inversion results.

Due to the absence of reliable weekly in situ measurements for comparison, we employed ERA5- and GLDAS-derived weekly $P-ET-R$ to validate the performance of weekly TWS changes derived from the three inversion solutions (GPD-mascon, GNSS, and joint inversion). It should be emphasized that the weekly P , ET , and R from ERA5 and GLDAS are the averages of hourly solutions. Before the comparison, we conducted an uncertainty assessment for the geodetic data inverted weekly dS_t/dt time series and hydrometeorological data derived weekly $P-ET-R$ time series, respectively. The uncertainties of weekly dS_t/dt time series derived from the GPD-mascon, GNSS, and joint inversion results (considering from error covariances, posterior error variances, and regularization parameters) are 30.81, 40.42, and 28.88 mm/week, respectively. This indicates that the reliability of the joint inversion results is higher than those of GPD-mascon and GNSS solutions. Meanwhile, the uncertainty of the weekly $P-ET-R$ time series estimated by the error propagation law (refer to the calculation method of Li et al. (2024)) is 10.36 mm/week, which is significantly smaller than those of geodetic inversion results. It

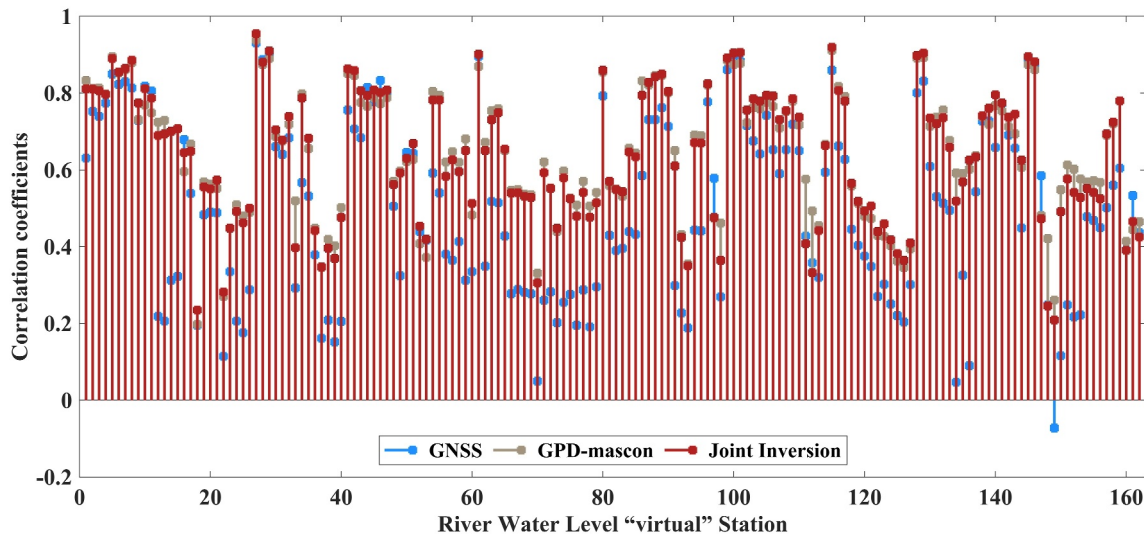


Figure 15. Changes in correlation coefficients between time series of monthly TWS changes from different inversion methods (GPD-mascon, GNSS, and joint inversion) and river water level observed by satellite altimetry at 162 “virtual” stations distributed in rivers within Brazil.

demonstrates that employing the ERA5- and GLDAS-derived weekly P-ET-R time series to validate the performance of weekly TWS changes derived from GPD-mascon, GNSS, and joint inversion solutions is justified. As the weekly TWS change time series are more complete and reliable before October 2014 (see Figure 13), Figure 16 depicts the weekly dS_t/dt time series from our three inversion results and ERA5-derived P-ET-R time series from January 2008 and October 2014. We can see that the P-ET-R and dS_t/dt time series maintain good consistency with each other and present significant seasonality. Table 3 lists the STDs and CCs between the time series of ERA5- and GLDAS-derived P-ET-R and dS_t/dt derived from three inversion results. As listed in Table 3, apart from a slightly lower consistency of the joint inversion results with ERA5-derived P-ET-R in southeastern Brazil compared to GPD-mascon solutions, the TWS change time series from joint inversion exhibit better consistency with ERA5- and GLDAS-derived P-ET-R time series across entire Brazil and its sub-regions than GPD-mascon and GNSS solutions. For instance, using the ERA5-derived P-ET-R as a reference, the solutions of joint inversion present a decrease of 5.19 mm/week and 3.11 mm/week in STDs and an increase of 11% and 5% in CCs compared to GNSS and GPD-mascon solutions over the entire Brazil. This suggests higher accuracy and reliability of our weekly joint inversion results. Additionally, since the monthly and weekly TWS change time series derived from our joint inversion model present better performance than the GNSS-only and GPD-mascon solutions, we used the non-seasonal components of the TWS change time series (deducting annual, semi-annual, and long-term signals) derived from the joint inversion in Figures 11a and 13a to investigate the 2009 extreme flood event in Brazil (see Text S4 and Figure S12 through Figure S14 in Supporting Information S1), the results demonstrate that the TWS change can effectively reveal the spatio-temporal evolutions of extreme flood events, and the weekly solutions provide more information on short-term scales compared to monthly solutions.

5. Conclusions

This study proposes a new joint inversion model for simultaneously inverting GRACE-based GPD observations and GNSS vertical displacements to obtain reliable TWS changes in Brazil from January 2008 to July 2016. The performance of the joint inversion results is evaluated through closed-loop simulations and external hydrometeorological data (P, ET, and R), as well as river water level data. Simulation analysis results indicate that the joint inversion results exhibit higher reliability in both temporal and spatial scales compared to GRACE-only (GPD-mascon) and GNSS-only solutions, and the mean STDs of joint results decrease by ~ 6.98 and ~ 37.5 mm compared to the results of GPD-mascon and GNSS (with a 3 mm noise level), respectively. For the inversion of measured data, our three inversion results (GPD-mascon, GNSS, and joint inversion) effectively reveal the monthly and weekly spatio-temporal evolution characteristics of TWS changes in Brazil during the study period, and present good consistency with the three official mascon solutions (CSR-M, JPL-M, and GSFC-M) and GFZ

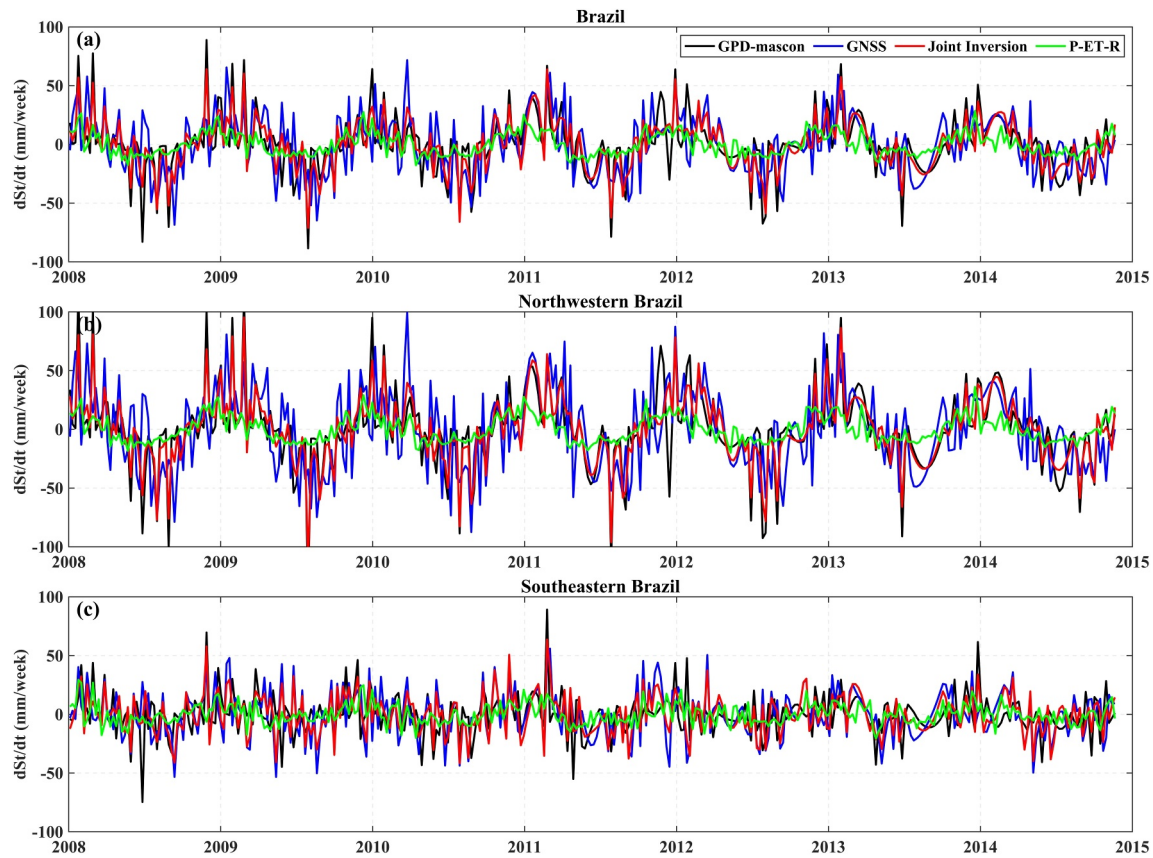


Figure 16. Comparison of weekly dS_t/dt time series derived from the solutions of GPD-mascon, GNSS, and joint inversion, as well as ERA5-derived P-ET-R time series in (a) Brazil and its (b) northwestern and (c) southeastern regions from January 2008 to October 2014.

SH solutions. Moreover, the joint inversion results show the smallest uncertainty (6.77 mm) compared to GNSS (34.71 mm) and GPD-mascon (8.89 mm) solutions in Brazil through the analysis of the GTCH method.

Additionally, at the monthly time scale, the R time series derived from the model-simulated P and ET combined with the jointly inverted TWS changes through the water budget closure method presents better consistency (STD = 19.607 mm and CC = 0.912) with in situ R time series at the Obidos hydrological station than those of

Table 3

Values of Standard Deviation (STD) of Residuals and Correlation Coefficient (CC) Between the Weekly dS_t/dt Time Series Derived From the Solutions of GNSS, GPD-Mascon, Joint Inversion, and the P-ET-R Time Series Derived From ERA5 and GLDAS in Brazil and Its Northwestern and Southeastern Regions From January 2008 to October 2014

Region	Data	ERA5 P-ET-R		GLDAS P-ET-R	
		STD (mm/week)	CC	STD (mm/week)	CC
Brazil	GNSS	22.49	0.49	22.25	0.49
	GPD-mascon	20.41	0.55	19.93	0.56
	Joint Inversion	17.30	0.60	16.82	0.61
Northwestern Brazil	GNSS	30.86	0.50	29.88	0.52
	GPD-mascon	28.17	0.56	26.96	0.59
	Joint Inversion	23.66	0.62	22.37	0.64
Southeastern Brazil	GNSS	19.30	0.29	19.23	0.31
	GPD-mascon	16.04	0.34	15.92	0.37
	Joint Inversion	15.99	0.33	15.73	0.38

GPD-mascon (STD = 20.879 mm and CC = 0.904) and GNSS (STD = 31.370 mm and CC = 0.778) solutions. Meanwhile, the joint solutions show better correlation with the river water level time series at 162 “virtual” stations observed by satellite altimetry compared to GPD-mascon and GNSS solutions. Furthermore, at the weekly time scale, the STDs and CCs between the joint inversion results and P-ET-R time series are superior to GPD-mascon solutions and significantly better than the GNSS estimates.

The joint inversion model effectively utilizes the respective strengths (spatio-temporal resolution, spatial coverage, and spectrum sensitivity) of GRACE and GNSS technologies in retrieving TWS changes, which constructs reliable TWS change time series with high spatio-temporal resolution in Brazil. Although the performance of the joint inversion model proposed in this work has only been evaluated in Brazil, it is also applicable to other regions observed with GNSS networks. Future investigations will further incorporate GRACE-FO data and focus on integrating other geodetic observations (e.g., Interferometric Synthetic Aperture Radar) with GRACE/GRACE-FO and GNSS through the multisource fusion method to obtain more reliable and stable TWS changes, which is of great significance for studying extreme climate changes and water cycle dynamics at global and regional scales.

Data Availability Statement

The GRACE-based geopotential difference (GPD) observations are available from Zhong et al. (2022). The GNSS vertical displacement time series are available from Blewitt et al. (2018). The geophysical fluid loading products published by the ESMGFZ are available from Dill and Dobslaw (2013). The CSR GRACE RL06 mascon solutions are available from Save et al. (2016), the JPL GRACE RL06 mascon solutions are available from Watkins et al. (2015), and the GSFC GRACE RL06 mascon solutions are available from Loomis et al. (2019). The monthly CSR SH and weekly GFZ SH solutions can be available at <https://icgem.gfz-potsdam.de/sl/temporal>. The precipitation (P), evapotranspiration (ET), and runoff (R) data provided by the Global Land Data Assimilation System (GLDAS) hydrologic model are available from Rodell et al. (2004). The ERA5 reanalysis data are available from Muñoz Sabater (2019), and the WGHM hydrological model is available from Müller et al. (2021). The river water level data provided by the Hydroweb are available from Silva et al. (2010).

Acknowledgments

This study was funded by the National Natural Science Foundation of China (42388102, 42374002, 42394132, and 41974015) and the Project Supported by the Special Fund of Hubei Luojia Laboratory (Grant 220100004). We would like to thank the editors and three anonymous reviewers for their insightful comments and suggestions that helped improve the quality of this manuscript.

References

- Adusumilli, S., Borsa, A. A., Fish, M. A., McMillan, H. K., & Silverii, F. (2019). A decade of water storage changes across the contiguous United States from GPS and satellite gravity. *Geophysical Research Letters*, 46(22), 13006–13015. <https://doi.org/10.1029/2019GL085370>
- Akaike, H. (1998). Likelihood and the Bayes procedure. In J. M. Bernardo, et al. (Eds.), *Bayesian statistics* (pp. 143–166). Univ. Press.
- Argus, D. F., Fu, Y., & Landerer, F. W. (2014). Seasonal variation in total water storage in California inferred from GPS observations of vertical land motion. *Geophysical Research Letters*, 41(6), 1971–1980. <https://doi.org/10.1002/2014GL059570>
- Argus, D. F., Martens, H. R., Borsa, A. A., Knappe, E., Wiese, D. N., Alam, S., et al. (2022). Subsurface water flux in California's Central Valley and its source watershed from space geodesy. *Geophysical Research Letters*, 49(22), e2022GL099583. <https://doi.org/10.1029/2022GL099583>
- Bettadpur, S. (2018). *UTCSR level-2 processing standards document (for level-2 product release 0006)* (Rev. 5.0, University of Texas at Austin, 2018. April 18, 2018) (pp. 327–742). GRACE Publication.
- Bevis, M., Alsdorf, D., Kendrick, E., Fortes, L. P., Forsberg, B., Smalley Jr, R., & Becker, J. (2005). Seasonal fluctuations in the mass of the Amazon River system and Earth's elastic response. *Geophysical Research Letters*, 32(16), L16308. <https://doi.org/10.1029/2005GL023491>
- Blewitt, G., Hammond, W. C., & Kreemer, C. (2018). Harnessing the GPS data explosion for interdisciplinary science. *Eos*, 99. <https://doi.org/10.1029/2018eo104623>
- Borsa, A. A., Agnew, D. C., & Cayan, D. R. (2014). Ongoing drought-induced uplift in the western United States. *Science*, 345(6204), 1587–1590. <https://doi.org/10.1126/science.1260279>
- Carlson, G., Werth, S., & Shirzaei, M. (2022). Joint inversion of GNSS and GRACE for terrestrial water storage change in California. *Journal of Geophysical Research: Solid Earth*, 127(3), e2021JB023135. <https://doi.org/10.1029/2021JB023135>
- Cazenave, A., Dominh, K., Guinehut, S., Berthier, E., Llovel, W., Ramillien, G., et al. (2009). Sea level budget over 2003–2008: A reevaluation from GRACE space gravimetry, satellite altimetry and Argo. *Global and Planetary Change*, 65(1–2), 83–88. <https://doi.org/10.1016/j.gloplacha.2008.10.004>
- Chambers, D. P. (2006). Observing seasonal steric sea level variations with GRACE and satellite altimetry. *Journal of Geophysical Research*, 111(C3), C03010. <https://doi.org/10.1029/2005JC002914>
- Chen, J., Tapley, B., Rodell, M., Seo, K. W., Wilson, C., Scanlon, B. R., & Pokhrel, Y. (2020). Basin-scale river runoff estimation from GRACE gravity satellites, climate models, and in situ observations: A case study in the Amazon basin. *Water Resources Research*, 56(10), e2020WR028032. <https://doi.org/10.1029/2020WR028032>
- Chen, J., Tapley, B., Save, H., Tamisiea, M. E., Bettadpur, S., & Ries, J. (2018). Quantification of ocean mass change using gravity recovery and climate experiment, satellite altimeter, and Argo floats observations. *Journal of Geophysical Research: Solid Earth*, 123(11), 10212–10225. <https://doi.org/10.1029/2018JB016095>
- Chen, J., Tapley, B., Tamisiea, M. E., Save, H., Wilson, C., Bettadpur, S., & Seo, K. W. (2021). Error assessment of GRACE and GRACE follow-on mass change. *Journal of Geophysical Research: Solid Earth*, 126(9), e2021JB022124. <https://doi.org/10.1029/2021JB022124>
- Chen, J. L., Wilson, C. R., & Tapley, B. D. (2006). Satellite gravity measurements confirm accelerated melting of Greenland ice sheet. *Science*, 313(5795), 1958–1960. <https://doi.org/10.1126/science.1129007>

- Chen, J. L., Wilson, C. R., Tapley, B. D., & Grand, S. (2007). GRACE detects coseismic and postseismic deformation from the Sumatra-Andaman earthquake. *Geophysical Research Letters*, 34(13), L13302. <https://doi.org/10.1029/2007GL030356>
- Dill, R., & Dobslaw, H. (2013). Numerical simulations of global-scale high-resolution hydrological crustal deformations. *Journal of Geophysical Research: Solid Earth*, 118(9), 5008–5017. <https://doi.org/10.1002/jgrb.50353>
- Dobslaw, H., Bergmann-Wolf, I., Dill, R., Forootan, E., Klemann, V., Kusche, J., & Sasgen, I. (2015). The updated ESA Earth System Model for future gravity mission simulation studies. *Journal of Geodesy*, 89(5), 505–513. <https://doi.org/10.1007/s00190-014-0787-8>
- Enzinger, T. L., Small, E. E., & Borsa, A. A. (2018). Accuracy of snow water equivalent estimated from GPS vertical displacements: A synthetic loading case study for western US mountains. *Water Resources Research*, 54(1), 581–599. <https://doi.org/10.1002/2017WR021521>
- Enzinger, T. L., Small, E. E., & Borsa, A. A. (2019). Subsurface water dominates Sierra Nevada seasonal hydrologic storage. *Geophysical Research Letters*, 46(21), 11993–12001. <https://doi.org/10.1029/2019GL084589>
- Farrell, W. E. (1972). Deformation of the Earth by surface loads. *Reviews of Geophysics*, 10(3), 761–797. <https://doi.org/10.1029/RG010i003p00761>
- Feng, W., Zhong, M., Lemoine, J. M., Biancale, R., Hsu, H. T., & Xia, J. (2013). Evaluation of groundwater depletion in North China using the Gravity Recovery and Climate Experiment (GRACE) data and ground-based measurements. *Water Resources Research*, 49(4), 2110–2118. <https://doi.org/10.1002/wrcr.20192>
- Ferreira, V., Yong, B., Montecino, H., Ndehedehe, C. E., Seitz, K., Kutterer, H., & Yang, K. (2023). Estimating GRACE terrestrial water storage anomaly using an improved point mass solution. *Scientific Data*, 10(1), 234. <https://doi.org/10.1038/s41597-023-02122-1>
- Ferreira, V. G., Ndehedehe, C. E., Montecino, H. C., Yong, B., Yuan, P., Abdalla, A., & Mohammed, A. S. (2019). Prospects for imaging terrestrial water storage in South America using daily GPS observations. *Remote Sensing*, 11(6), 679. <https://doi.org/10.3390/rs11060679>
- Fok, H. S., & Liu, Y. (2019). An improved GPS-inferred seasonal terrestrial water storage using terrain-corrected vertical crustal displacements constrained by GRACE. *Remote Sensing*, 11(12), 1433. <https://doi.org/10.3390/rs11121433>
- Fu, Y., Argus, D. F., & Landerer, F. W. (2015). GPS as an independent measurement to estimate terrestrial water storage variations in Washington and Oregon. *Journal of Geophysical Research: Solid Earth*, 120(1), 552–566. <https://doi.org/10.1002/2014JB011415>
- Golub, G. H., Heath, M., & Wahba, G. (1979). Generalized cross-validation as a method for choosing a good ridge parameter. *Technometrics*, 21(2), 215–223. <https://doi.org/10.1080/00401706.1979.10489751>
- Han, S. C., & Rzeghzi, S. M. (2017). GPS recovery of daily hydrologic and atmospheric mass variation: A methodology and results from the Australian continent. *Journal of Geophysical Research: Solid Earth*, 122(11), 9328–9343. <https://doi.org/10.1002/2017JB014603>
- Han, S. C., Shum, C. K., & Braun, A. (2005). High-resolution continental water storage recovery from low-low satellite-to-satellite tracking. *Journal of Geodynamics*, 39(1), 11–28. <https://doi.org/10.1016/j.jog.2004.08.002>
- Han, S. C., Shum, C. K., & Jekeli, C. (2006). Precise estimation of in situ geopotential differences from GRACE low-low satellite-to-satellite tracking and accelerometer data. *Journal of Geophysical Research*, 111(B4), 1–13. <https://doi.org/10.1029/2005JB003719>
- Huang, W., Duan, W., & Chen, Y. (2021). Rapidly declining surface and terrestrial water resources in Central Asia driven by socio-economic and climatic changes. *Science of the Total Environment*, 784, 147193. <https://doi.org/10.1016/j.scitotenv.2021.147193>
- Humphrey, V., Gudmundsson, L., & Seneviratne, S. I. (2016). Assessing global water storage variability from GRACE: Trends, seasonal cycle, subseasonal anomalies and extremes. *Surveys in Geophysics*, 37(2), 357–395. <https://doi.org/10.1007/s10712-016-9367-1>
- Jacob, T., Wahr, J., Pfeffer, W. T., & Swenson, S. (2012). Recent contributions of glaciers and ice caps to sea level rise. *Nature*, 482(7386), 514–518. <https://doi.org/10.1038/nature10847>
- Jiang, Z., Hsu, Y. J., Yuan, L., Cheng, S., Feng, W., Tang, M., & Yang, X. (2022). Insights into hydrological drought characteristics using GNSS-inferred large-scale terrestrial water storage deficits. *Earth and Planetary Science Letters*, 578, 117294. <https://doi.org/10.1016/j.epsl.2021.117294>
- Jiang, Z., Hsu, Y. J., Yuan, L., Cheng, S., Li, Q., & Li, M. (2021). Estimation of daily hydrological mass changes using continuous GNSS measurements in mainland China. *Journal of Hydrology*, 598, 126349. <https://doi.org/10.1016/j.jhydrol.2021.126349>
- Kim, J. S., Seo, K. W., Kim, B. H., Ryu, D., Chen, J., & Wilson, C. (2024). High-resolution terrestrial water storage estimates from GRACE and land surface models. *Water Resources Research*, 60(2), e2023WR035483. <https://doi.org/10.1029/2023WR035483>
- Koch, K. R., & Kusche, J. (2002). Regularization of geopotential determination from satellite data by variance components. *Journal of Geodesy*, 76(5), 259–268. <https://doi.org/10.1007/s00190-002-0245-x>
- Kusche, J. E. J. O., & Schrama, E. J. O. (2005). Surface mass redistribution inversion from global GPS deformation and Gravity Recovery and Climate Experiment (GRACE) gravity data. *Journal of Geophysical Research*, 110(B9), B09409. <https://doi.org/10.1029/2004JB003556>
- Landerer, F. (2019). *Monthly estimates of degree-1 (geocenter) gravity coefficients, generated from GRACE (04-2002-06/2017) and GRACEFO (06/2018 onward) RL06 solutions*. GRACE Technical Note 13, the GRACE Project, NASA Jet Propulsion Laboratory.
- Lehner, B., Döll, P., Alcamo, J., Henrichs, T., & Kaspar, F. (2006). Estimating the impact of global change on flood and drought risks in Europe: A continental, integrated analysis. *Climatic Change*, 75(3), 273–299. <https://doi.org/10.1007/s10584-006-6338-4>
- Li, X., Zhong, B., Chen, J., Li, J., & Wang, H. (2024). Investigation of 2020–2022 extreme floods and droughts in Sichuan Province of China based on joint inversion of GNSS and GRACE/GFO data. *Journal of Hydrology*, 632, 130868. <https://doi.org/10.1016/j.jhydrol.2024.130868>
- Li, X., Zhong, B., Li, J., & Liu, R. (2023a). Joint inversion of GNSS and GRACE/GFO data for terrestrial water storage changes in the Yangtze River Basin. *Geophysical Journal International*, 233(3), 1596–1616. <https://doi.org/10.1093/gji/ggad014>
- Li, X., Zhong, B., Li, J., & Liu, R. (2023b). Inversion of terrestrial water storage changes from GNSS vertical displacements using a priori constraint: A case study of the Yunnan Province, China. *Journal of Hydrology*, 617, 129126. <https://doi.org/10.1016/j.jhydrol.2023.129126>
- Long, D., Longuevergne, L., & Scanlon, B. R. (2014). Uncertainty in evapotranspiration from land surface modeling, remote sensing, and GRACE satellites. *Water Resources Research*, 50(2), 1131–1151. <https://doi.org/10.1002/2013WR014581>
- Long, D., Scanlon, B. R., Longuevergne, L., Sun, A. Y., Fernando, D. N., & Save, H. (2013). GRACE satellite monitoring of large depletion in water storage in response to the 2011 drought in Texas. *Geophysical Research Letters*, 40(13), 3395–3401. <https://doi.org/10.1002/grl.50655>
- Loomis, B. D., Luthcke, S. B., & Sabaka, T. J. (2019). Regularization and error characterization of GRACE mascons. *Journal of Geodesy*, 93(9), 1381–1398. <https://doi.org/10.1007/s00190-019-01252-y>
- Loomis, B. D., Rachlin, K. E., Wiese, D. N., Landerer, F. W., & Luthcke, S. B. (2020). Replacing GRACE/GRACE-FO with satellite laser ranging: Impacts on Antarctic Ice Sheet mass change. *Geophysical Research Letters*, 47(3), e2019GL085488. <https://doi.org/10.1029/2019GL085488>
- Luo, H., Liu, Y., Chen, T., Xu, C., & Wen, Y. (2016). Derivation of 3-D surface deformation from an integration of InSAR and GNSS measurements based on Akaike's Bayesian Information Criterion. *Geophysical Journal International*, 204(1), 292–310. <https://doi.org/10.1093/gji/ggv453>
- Milliner, C., Materna, K., Bürgmann, R., Fu, Y., Moore, A. W., Bekaert, D., et al. (2018). Tracking the weight of Hurricane Harvey's stormwater using GPS data. *Science Advances*, 4(9), eaau2477. <https://doi.org/10.1126/sciadv.aau2477>

- Müller Schmied, H., Cáceres, D., Eisner, S., Flörke, M., Herbert, C., Niemann, C., et al. (2021). The global water resources and use model WaterGAP v2. 2d: Model description and evaluation. *Geoscientific Model Development*, 14(2), 1037–1079. <https://doi.org/10.5194/gmd-14-1037-2021>
- Muñoz Sabater, J. (2019). ERA5-Land monthly averaged data from 1950 to present. *Copernicus Climate Change Service (C3S) Climate Data Store (CDS)*. <https://doi.org/10.24381/cds.68d2bb30>. Accessed on 20-08-2023.
- Peltier, W. R., Argus, D. F., & Drummond, R. (2018). Comment on “An assessment of the ICE-6G_C (VM5a) glacial isostatic adjustment model” by Purcell et al. *Journal of Geophysical Research: Solid Earth*, 123(2), 2019–2028. <https://doi.org/10.1002/2016JB013844>
- Pokhrel, Y., Felfelani, F., Satoh, Y., Boulange, J., Burek, P., Gädeke, A., et al. (2021). Global terrestrial water storage and drought severity under climate change. *Nature Climate Change*, 11(3), 226–233. <https://doi.org/10.1038/s41558-020-00972-w>
- Premoli, A., & Tavella, P. (1993). A revisited three-cornered hat method for estimating frequency standard instability. *IEEE Transactions on Instrumentation and Measurement*, 42(1), 7–13. <https://doi.org/10.1109/19.206671>
- Ramillien, G., Biancale, R., Gratton, S., Vasseur, X., & Bourgogne, S. (2011). GRACE-derived surface water mass anomalies by energy integral approach: Application to continental hydrology. *Journal of Geodesy*, 85(6), 313–328. <https://doi.org/10.1007/s00190-010-0438-7>
- Razeghi, M., Han, S. C., McClusky, S., & Sauber, J. (2019). A joint analysis of GPS displacement and GRACE geopotential data for simultaneous estimation of geocenter motion and gravitational field. *Journal of Geophysical Research: Solid Earth*, 124(11), 12241–12263. <https://doi.org/10.1029/2019JB018289>
- Rietbroek, R., Fritsche, M., Brunnabend, S. E., Daras, I., Kusche, J., Schröter, J., et al. (2012). Global surface mass from a new combination of GRACE, modelled OBP and reprocessed GPS data. *Journal of Geodynamics*, 59, 64–71. <https://doi.org/10.1016/j.jog.2011.02.003>
- Rodell, M., Houser, P. R., Jambor, U. E. A., Gottschalk, J., Mitchell, K., Meng, C. J., et al. (2004). The global land data assimilation system. *Bulletin of the American Meteorological Society*, 85(3), 381–394. <https://doi.org/10.1175/BAMS-85-3-381>
- Rodell, M., Velicogna, I., & Famiglietti, J. S. (2009). Satellite-based estimates of groundwater depletion in India. *Nature*, 460(7258), 999–1002. <https://doi.org/10.1038/nature08238>
- Save, H., Bettadpur, S., & Tapley, B. D. (2016). High-resolution CSR GRACE RL05 mascons. *Journal of Geophysical Research: Solid Earth*, 121(10), 7547–7569. <https://doi.org/10.1002/2016JB013007>
- Shang, K., Guo, J., Shum, C. K., Dai, C., & Luo, J. (2015). GRACE time-variable gravity field recovery using an improved energy balance approach. *Geophysical Journal International*, 203(3), 1773–1786. <https://doi.org/10.1093/gji/ggv392>
- Silva, J. S. D., Calmant, S., Seyler, F., Rotunno Filho, O. C., Cochonneau, G., & Mansur, W. J. (2010). Water levels in the Amazon basin derived from the ERS 2 and ENVISAT radar altimetry missions. *Remote Sensing of Environment*, 114(10), 2160–2181. <https://doi.org/10.1016/j.rse.2010.04.020>
- Syed, T. H., Famiglietti, J. S., Rodell, M., Chen, J., & Wilson, C. R. (2008). Analysis of terrestrial water storage changes from GRACE and GLDAS. *Water Resources Research*, 44(2), W02433. <https://doi.org/10.1029/2006WR005779>
- Tangdamrongsak, N., Hwang, C., Shum, C. K., & Wang, L. (2012). Regional surface mass anomalies from GRACE KBR measurements: Application of L-curve regularization and a priori hydrological knowledge. *Journal of Geophysical Research*, 117(B11), B11406. <https://doi.org/10.1029/2012JB009310>
- Tapley, B. D., Watkins, M. M., Flechtner, F., Reigber, C., Bettadpur, S., Rodell, M., et al. (2019). Contributions of GRACE to understanding climate change. *Nature Climate Change*, 9(5), 358–369. <https://doi.org/10.1038/s41558-019-0456-2>
- Thomas, A. C., Reager, J. T., Famiglietti, J. S., & Rodell, M. (2014). A GRACE-based water storage deficit approach for hydrological drought characterization. *Geophysical Research Letters*, 41(5), 1537–1545. <https://doi.org/10.1002/2014GL059323>
- van Dam, T., Wahr, J., & Lavallée, D. (2007). A comparison of annual vertical crustal displacements from GPS and Gravity Recovery and Climate Experiment (GRACE) over Europe. *Journal of Geophysical Research*, 112(B3), B03404. <https://doi.org/10.1029/2006JB004335>
- Wahr, J., Khan, S. A., van Dam, T., Liu, L., van Angelen, J. H., van den Broeke, M. R., & Meertens, C. M. (2013). The use of GPS horizontals for loading studies, with applications to northern California and southeast Greenland. *Journal of Geophysical Research: Solid Earth*, 118(4), 1795–1806. <https://doi.org/10.1002/jgrb.50104>
- Wahr, J., Molenaar, M., & Bryan, F. (1998). Time variability of the Earth's gravity field: Hydrological and oceanic effects and their possible detection using GRACE. *Journal of Geophysical Research*, 103(B12), 30205–30229. <https://doi.org/10.1029/98JB02844>
- Wang, H., Xiang, L., Jia, L., Jiang, L., Wang, Z., Hu, B., & Gao, P. (2012). Load Love numbers and Green's functions for elastic Earth models PREM, iasp91, ak135, and modified models with refined crustal structure from Crust 2.0. *Computers & Geosciences*, 49, 190–199. <https://doi.org/10.1016/j.cageo.2012.06.022>
- Wang, S. Y., Li, J., Chen, J., & Hu, X. G. (2022). On the improvement of mass load inversion with GNSS horizontal deformation: A synthetic study in Central China. *Journal of Geophysical Research: Solid Earth*, 127(10), e2021JB023696. <https://doi.org/10.1029/2021JB023696>
- Watkins, M. M., Wiese, D. N., Yuan, D. N., Boening, C., & Landerer, F. W. (2015). Improved methods for observing Earth's time variable mass distribution with GRACE using spherical cap mascons. *Journal of Geophysical Research: Solid Earth*, 120(4), 2648–2671. <https://doi.org/10.1002/2014JB011547>
- White, A. M., Gardner, W. P., Borsa, A. A., Argus, D. F., & Martens, H. R. (2022). A review of GNSS/GPS in hydrogeodesy: Hydrologic loading applications and their implications for water resource research. *Water Resources Research*, 58(7), e2022WR032078. <https://doi.org/10.1029/2022WR032078>
- Wu, D., Yan, H., & Shen, Y. (2017). TSAAnalyzer, a GNSS time series analysis software. *GPS Solutions*, 21(3), 1389–1394. <https://doi.org/10.1007/s10291-017-0637-2>
- Wu, X., Hefflin, M. B., Ivins, E. R., & Fukumori, I. (2006). Seasonal and interannual global surface mass variations from multisatellite geodetic data. *Journal of Geophysical Research*, 111(B9), B09401. <https://doi.org/10.1029/2005JB004100>
- Yang, X., Yuan, L., Jiang, Z., Tang, M., Feng, X., & Li, C. (2023). Investigating terrestrial water storage changes in Southwest China by integrating GNSS and GRACE/GRACE-FO observations. *Journal of Hydrology: Regional Studies*, 48, 101457. <https://doi.org/10.1016/j.ejrh.2023.101457>
- Zhang, T., & Jin, S. (2016). Evapotranspiration variations in the Mississippi River Basin estimated from GPS observations. *IEEE Transactions on Geoscience and Remote Sensing*, 54(8), 4694–4701. <https://doi.org/10.1109/TGRS.2016.2549364>
- Zhong, B., Li, Q., Chen, J., & Luo, Z. (2022). A dataset of GRACE intersatellite geopotential differences from April 2002 to July 2016 (version V2) [Dataset]. *Science Data Bank*. <https://doi.org/10.11922/sciencedb.j00001.00365>
- Zhong, B., Li, Q., Chen, J., Luo, Z., & Zhou, H. (2020). Improved estimation of regional surface mass variations from GRACE intersatellite geopotential differences using a priori constraints. *Remote Sensing*, 12(16), 2553. <https://doi.org/10.3390/rs12162553>
- Zhong, B., Li, Q., Li, X., & Chen, J. (2023). Basin-scale terrestrial water storage changes inferred from GRACE-based geopotential differences: A case study of the Yangtze River Basin, China. *Geophysical Journal International*, 233(2), 1318–1338. <https://doi.org/10.1093/gji/ggac524>

- Zhu, H., Chen, K., Hu, S., Liu, J., Shi, H., Wei, G., et al. (2023). Using the global navigation satellite system and precipitation data to establish the propagation characteristics of meteorological and hydrological drought in Yunnan, China. *Water Resources Research*, 59(4), e2022WR033126. <https://doi.org/10.1029/2022WR033126>
- Zhu, H., Chen, K., Hu, S., Wei, G., Chai, H., & Wang, T. (2023). Characterizing hydrological droughts within three watersheds in Yunnan, China from GNSS-inferred terrestrial water storage changes constrained by GRACE data. *Geophysical Journal International*, 235(2), 1581–1599. <https://doi.org/10.1093/gji/ggad321>